UNCERTAINTY ON MEASUREMENT OF ELASTOMERIC ISOLATORS EFFECTIVE PROPERTIES

Sebastián Miranda[1,3], Juan Carlos de la Llera[1], and Eduardo Miranda[2]

[1]Departament of Structural and Geotechnical Engineering, Pontificia Universidad Catolica de Chile, and National Research Center for Integrated Natural Disaster Management, CONICYT/FONDAP/15110017, Santiago 7820436, Chile

[2] John A. Blume Earthquake Engineering Center, Department of Civil and Environmental Engineering, Stanford University, Stanford, CA 94305-4020, U.S.A.

[3] Faculty of Engineering, Universidad del Desarrollo, Santiago, Chile.

ABSTRACT

Elastomeric isolators are subjected to a series of non-destructive tests with several repeated deformation cycles. For each cycle, effective properties are calculated and afterward averaged. Despite their variability, and therefore their inherent uncertainties, these properties are treated as deterministic values by seismic design procedures. In this research, these uncertainties are quantified, based on the *Guide to the expression of Uncertainty in Measurement*, *GUM*, and Monte-Carlo simulations, considering variability between repetitions and instrumentation errors. Uncertainties were calculated for a dataset of 2,498 isolators' test results, finding that the maximum relative expanded uncertainty was 12%. The *GUM* and Monte-Carlo methods lead to similar results, and higher-order effects in the *GUM* assessment were negligible. A comprehensive analysis to evaluate the influence of the directly-measured quantities in the properties uncertainties was performed. Results showed that forces and displacements measurement errors are equally relevant in stiffness uncertainties, but force measurement errors primarily control damping uncertainties.

KEYWORDS

Seismic isolation properties, uncertainty in measurements, *GUM* methodology, Monte-Carlo methods.

1. Introduction

Elastomeric seismic isolators are manufactured from several thin layers of natural or synthetic rubber intercalated with thin steel plates. Due to isolators' horizontal flexibility, the isolated structure response is uncoupled from the ground motion excitation. Isolators also provide the required strength and stiffness to withstand the vertical loads. Based on the inherent variability of rubber mechanical properties and uncertainties arising in the fabrication process, as isolators are frequently custom designed and manufactured, seismic codes (e.g., ASCE/SEI 7-16 [1], NCh2745 [2]) establish rigorous testing programs for prototype and production isolators with standard loading protocols. Results from these tests show that elastomeric isolators present a strongly nonlinear force-displacement relationship, including axial load dependency, strain hardening, strain-rate effects, and load-path effects. Moreover, the widely studied Mullins effect [3], which corresponds to a degradation of the isolator maximum load and stiffness after each load cycle (a phenomenon also referred to as *scragging or softening*), is also observed. To account for these isolators' mechanical features, tests consider several displacement sequences at a given shear deformation. For each sequence, several fully-reversed displacement cycles are performed. A typical shear force-lateral displacement curve for an elastomeric isolator is shown in Figure 1 at four different normalized levels of shear deformation $\gamma = 0.25, 0.50, 1.0$ and 1.5. In this context, the normalized deformation is defined as the ratio between the lateral deformation and the isolators' total rubber thickness. Full cycles are presented in Figure 1(a), and a close-up of the maximum forces is shown in Figure 1(b).

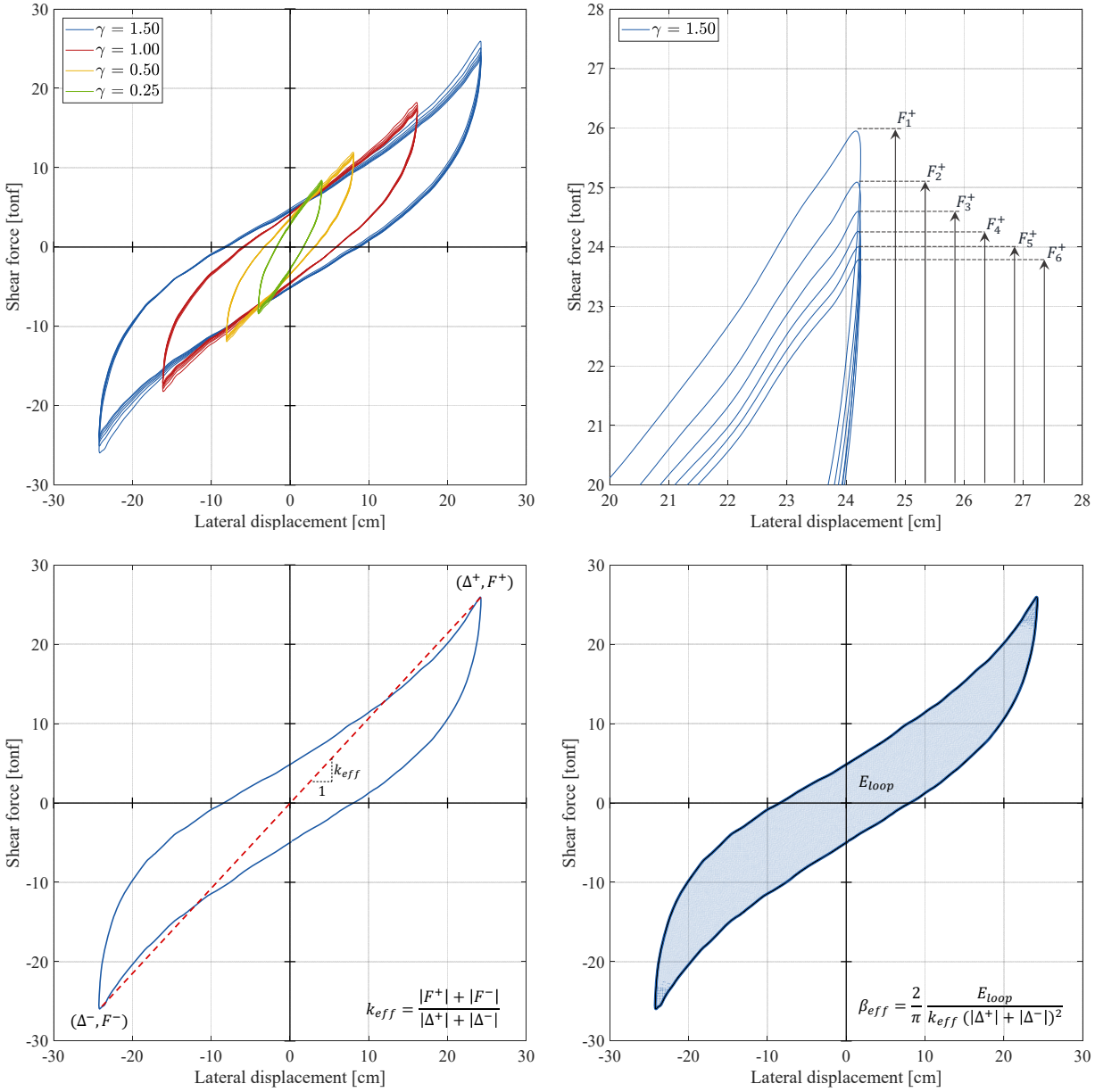

Figure 1(a) Shear force – lateral displacement hysteretic curve for Specimen 1, as described below, considering four displacement sequences with $\gamma = 0.25, 0.50, 1.00$, and 1.50 and six repetition cycles for each level of deformation; (b) Different maximum force values used for uncertainty calculation; (c) Equivalent secant stiffness k_{eff} as defined in ASCE-7 and NCh2745; and (d) Energy dissipated in one cycle, E_{loop}, as required for equivalent damping β_{eff} calculation (tonf = 9.81 kN)

Despite the complexity of elastomeric isolators' behavior, most structures are designed using an approximate methodology based on only two effective isolator properties derived from parameters obtained from measured-by-test shear force - lateral displacement hysteretic curves; which are: (1) the lateral effective secant stiffness k_{eff}, calculated as the force-displacement secant stiffness corresponding to a specific (objective) displacement, (Figure 1(c)), and (2) the effective viscous damping ratio β_{eff}, based on the energy dissipated through hysteretic behavior (E_{loop}) during a full cycle of reversible load over the total displacement amplitude $|\Delta^+| + |\Delta^-|$ [4], as it is schematically shown in Figure 2(d) and presented elsewhere [5]. Effective stiffness k_{eff} and effective damping β_{eff} are calculated for each level of lateral deformation and their values averaged across the various cycles at that level of deformation, discarding

the first cycle to use the so-called *scragged properties* of the isolator. The acceptance or rejection of a specific isolator unit is based on its average properties, thus neglecting these derived parameters' cycle-to-cycle variability and their associated uncertainties.

Variability in measurements is a relevant topic since the measurand value by itself does not constitute a complete test result [6]. It should be mandatory to specify the quality of the result with a parameter that reflects its variability; however, this information is frequently skipped in reporting test results. For example, variability in structural elements' mechanical properties leads to an increase in the uncertainty of the structural responses estimated using those measured properties. Several uncertainty calculation procedures have been proposed and used historically [7]. However, since the release of the *Guide to the Expression of Uncertainty in Measurement (GUM)* [8], the testing industry has embraced this methodology as a standard. The publication of this *Guide* constitutes a landmark in the measurement field, as it presented, probably for the first time, a comprehensive and standardized approach for uncertainty quantification, evaluation, and propagation irrespective of the type of measurement and the required level of accuracy [9]. The *Guide* uses a first-order Taylor series expansion for estimating the variance of an arbitrary output quantity y, i.e., the test measurand, as a function of the variances of n input quantities x_i, which are directly measured or estimated during the test. The measurand y and the input quantities x_i need to be related through a model $y = f(x_1, x_2, \dots, x_n)$. The *Guide* uses both, frequentist and Bayesian statistical methods, to assign a standard uncertainty value for each of the input quantities x_i and then propagate them into the measurand y. Also, the *Guide* includes supplements for Monte-Carlo implementation [10], a glossary of metrology-related concepts, the International vocabulary of Metrology *VIM* [6], and other related documents.

Da Silva and Ten Caten [11] presented a comprehensive literature review comprising 114 journal articles published in four journals between 2004 and 2010 in which the main topic was measurement uncertainty. The authors classified the articles based on different criteria, one of them being the method used for uncertainty quantification. By far, the most commonly used technique was the *GUM* method, followed by Monte-Carlo simulation and Fuzzy variables procedures [12,13]. This research focuses on the evaluation of uncertainty in the effective properties of elastomeric isolation bearings using the *GUM* methodology and Monte-Carlo simulation.

Many research articles in vastly different fields assessing uncertainty using the *GUM* procedure are available in the literature. For instance, Shahanaghi and Nakhjiri [14] quantified the uncertainty in the calibration of a platinum resistance thermometer using the *GUM* methodology and Monte-Carlo simulation, and results showed a difference between the symmetric uncertainty interval obtained with *GUM* and a skewed uncertainty interval given by Monte-Carlo simulation. Both approaches were also implemented in the work of Theodorou et al. [15] in the evaluation of the uncertainty in the direct estimation of cadmium in water by graphite furnace atomic absorption spectrometry. Their results showed a mild overestimation of the uncertainty when the *GUM* method was implemented. Chen and Chen [16] assessed the uncertainty on a perspiration measurement system composed of several sensors, considering several uncertainty sources as airflow rate, air density, and humidity. The authors compared *GUM* and Monte-Carlo methods obtaining no significant differences in the uncertainty values. Junga et al. [17] quantified the uncertainties of the measurements required to determine the thermal-balance in small-scale boilers, also implementing both methodologies. The authors concluded that Monte-Carlo methods are faster, simpler, and easier to implement in spreadsheets of commercial computation tools, delivering results showing excellent accuracy relative to the ones from the *GUM* method. In the recent work of Moona et al. [18], the dot pitch of a display monitor shadow mask was measured by interferometry. Again, they assessed the uncertainty of the expected dot pitch value by the GUM and Monte-Carlo methods, obtaining similar values for both approaches. Tutmez and Baranovski [19] studied the uncertainty of railway noise measurements, considering sources arising from instrumentation, calibration, operation bias, and random variability, finding that randomness was the most relevant uncertainty source. The authors also proposed a methodology to determine the optimum measurement instrument position.

Some relevant articles in civil and mechanical engineering applications include the work of Link et al. [20] and Bringmann and Knapp [21] that used Monte-Carlo simulation to assess the uncertainty on the parameters characterizing piezoelectric accelerometers, and on the measurements performed during a machine tool calibration, respectively. Furthermore, the work of Leyi et al. [22] analyzed uncertainty sources for Brinell hardness measurements. Additionally, they used finite elements and Monte-Carlo simulations to acquire theoretical measurement uncertainties. Mahmoud and Hegazy [23] implemented the *GUM* and Monte-Carlo methods to assess Brinell and Vickers hardness measurements' uncertainty. As in previous investigations, their results showed no significant differences between the *GUM* expanded uncertainty and the Monte-Carlo evaluation. Also, they found that the correlations between input quantities play an essential role in the estimated uncertainties. Kuhinek et al. [24]

studied uniaxial compressive tests of rock samples to determine their strength and deformability. They performed a *GUM* uncertainty assessment, considering transducers and other instruments as sources of uncertainty. Results showed a relative standard uncertainty lower than 1% for strength and elasticity modulus, and ranging from 2.6% to 12% for the Poisson coefficient. In this investigation field, Tutmez [25] performed an uncertainty analysis of rocks' dynamic elastic properties, measured by ultrasonic wave propagation. The author compared the results of several methods, including *GUM,* Monte-Carlo, and Copula-based analysis, concluding that Monte-Carlo is an effective way to assess uncertainties, though it requires full probability distributions for all input quantities. On the other hand, the Copula-based method considers the correlations among the input quantities through a joint probability distribution. Godina and Acko [26] analyzed the calibration of a gauge block, comparing the interferometric and mechanical methods for calibration. They concluded that mechanical calibration delivers expected values that are reliable but still more uncertain than the ones estimated with interferometric calibration. Additionally, Salah et al. [27] presented an uncertainty analysis of stress and elongation measurement on metal tensile tests by implementing the *GUM* method, Monte-Carlo simulation, and Markov Chain Monte-Carlo simulation. Kapper et al. [28] studied plastic anisotropy ratio for sheet-metals finding that the most relevant sources of uncertainty were repeatability and reproducibility, being the latter more significant than the former. As defined in the *GUM* [8], repeatability considers independent test results obtained from nominally identical specimens tested with the same method, same laboratory, same equipment, and same operator, while reproducibility considers the same testing method done on nominally identical specimens but performed by different operators, different equipment, and/or different laboratories.

The main objectives of this research are: (1) to implement an uncertainty quantification procedure for the measured-by-test effective properties of elastomeric seismic isolators, according to the *GUM* methodology; (2) to evaluate the uncertainty on the effective properties considering only Type A (repeatability) uncertainty sources; (3) to evaluate the uncertainty on the effective properties considering combined Type A and Type B sources of uncertainty; (4) to validate the results from GUM methodology by using Monte-Carlo simulation; and (5) to study the relative relevance of the different uncertainty sources in the uncertainties of the effective properties.

2. Uncertainty Evaluation Procedures

2.1 Elastomeric Isolators Test-Results Dataset

This research project was developed in conjunction with the "Laboratory for dynamic testing and vibration control" at Pontificia Universidad Catolica de Chile. This testing facility has performed more than 6,000 tests of elastomeric seismic isolators during the last twenty years. For further details on the experimental test setup, the reader is referred to De la Llera et al. [29]. As required by the seismic isolation Chilean Code NCh2745 [2], two types of experimental tests are performed: (i) prototype tests, applied over a representative sample of the isolators of the project to validate the isolation system design properties considering several combinations of dead loads, live loads, wind loads and earthquake loads; and (ii) quality-control tests (production tests in ASCE/SEI 7-16 [1] terminology) in which all the seismic isolators of the project are subjected to consecutive sequences of lateral deformation, typically at values of shear strain $\gamma = 0.25$, $\gamma = 0.50$, $\gamma = 1.00$, and at a final design value $\gamma = \gamma_D$, as defined by the structural engineer, which usually ranges between $\gamma = 1.20$ and $\gamma = 1.50$ for the Chilean design experience. All these shear strains are simultaneously imposed under the expected axial load, i.e., the average axial load for all isolators of the same type under the dead (D), and live (L) loads, using a load combination of D + 0.50 L.

The dataset used in this study considered the results of more than 2,400 quality-control tests of elastomeric seismic isolators from 40 projects constructed between 2007 and 2014 in Chile and Peru. These projects include hospitals, buildings, bridges, and various types of industrial facilities. All specimens were manufactured by the same company, using two different vulcanized natural rubber compounds, namely, Compound 1, for low stiffness seismic isolators, and Compound 2, for medium stiffness seismic isolators. All specimens have annular geometry with external diameters (D_{ext}) ranging from 50 cm to 115 cm, internal diameters (D_{int}) from 10 cm to 15 cm, 0.3 cm thick steel shims (t_s), and 2 cm thick end steel plates (e_s) at the top and bottom. Isolator total rubber heights range from 12.6 cm to 25.9 cm, using rubber layers with thicknesses (t_r) ranging from 0.6 cm to 0.8 cm. The expected axial loads over the isolators range from 3760 kN to 10380 kN, and from 1960 kN to 9200 kN, implying vertical stresses ranging from 2.1 MPa to 20.2 MPa, and from 5.5 MPa to 16.800 MPa for compounds 1 and 2, respectively. Table 1 classifies the specimens based on their manufacturing compound and external diameter. Figure 2 shows the geometric parameters of an isolator unit.

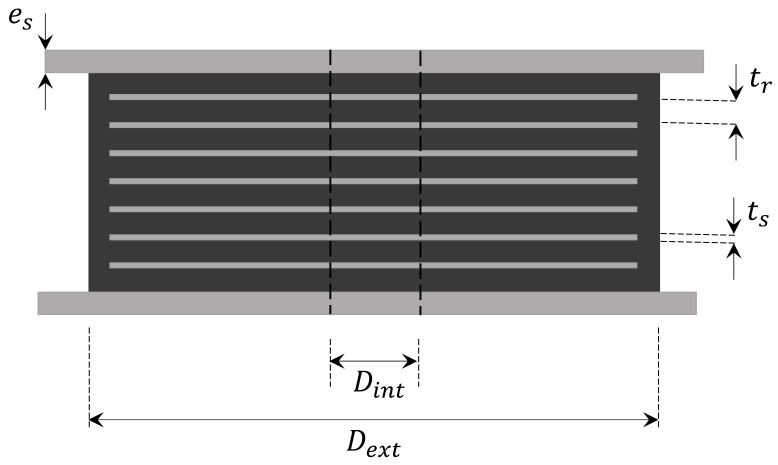

Figure 2. Seismic isolator geometric parameters.

Table 1. Number of isolators and main geometric features

	Number of Specimens	
Isolator External Diameter (cm)	Compound 1	Compound 2
50	0	13
60	148	13
65	56	130
70	38	539
75	409	219
80	62	197
85	33	76
90	227	175
100	91	27
115	45	0
Total	**1109**	**1389**

2.2 Summary of the GUM Uncertainty Quantification Methodology

The *GUM* methodology for measurement uncertainty assessment has become the standard in the last decades, mainly because of its simplicity and ability to combine different sources of uncertainty. Uncertainties assessed from several measurements under *repeatability conditions*, and uncertainties evaluated from non-statistically assessed data, are defined as Type A and Type B sources of uncertainty, respectively. Type B uncertainty sources are related to code tolerances, experience values, instrument resolution, variability in operators, among others.

Given some functional relationship between an arbitrary number of assumed uncorrelated input quantities x_i, which are in most cases directly measured, and an output quantity computed from measured quantities $y = f(x_1, x_2, \dots, x_n)$, the combined uncertainty on the output quantity $u_c(y)$ is estimated by propagating the uncertainties in the input quantities $u(x_i)$ through the expression:

$$u_c{}^2(y) = \sum_{i=1}^{N} \left(\frac{\partial f}{\partial x_\mathrm{i}}\right)^2 u^2(x_\mathrm{i}) \tag{1}$$

This equation is based on a first-order Taylor series expansion of the variance of the measurand model for measurand y. As stated in the *Guide* [8], the combined uncertainty $u_c{}^2(y)$ is an estimator of the variance and characterizes the dispersion of the values that could be reasonably be attributed to the measurand Y. It should be noted, that Equation

(1) only applies when all the input quantities x_i are mutually uncorrelated. The partial derivatives are typically named sensitivity coefficients

$$c_i = \partial f / \partial x_i = \partial y / \partial x_i \tag{2}$$

Equation (1) can be conveniently rewritten in matrix format as

$$u_c{}^2(y) = \boldsymbol{g}^T \boldsymbol{u^2}(x_i) \boldsymbol{g} \tag{3}$$

where

$$\boldsymbol{g} = \left[\frac{\partial y}{\partial x_1} \quad \frac{\partial y}{\partial x_2} \quad \dots \quad \frac{\partial y}{\partial x_n}\right]^{\boldsymbol{T}} = \boldsymbol{\nabla} y \tag{4}$$

is a gradient vector containing the sensitivity coefficients of the measurand $y = f(x_1, x_2, \dots, x_n)$ with respect to all the input variables x_i and

$$\boldsymbol{u^2}(x_i) = \begin{bmatrix} u^2(x_1) & 0 & \dots & 0 \\ 0 & u^2(x_2) & \dots & 0 \\ \vdots & \vdots & \ddots & \vdots \\ 0 & 0 & \dots & u^2(x_n) \end{bmatrix} \tag{5}$$

is a diagonal matrix where $u^2(x_i)$ is the squared standard uncertainty for each input quantity x_i.

The counterpart of Equation (1) for the case with correlated input quantities, a frequent condition in measuring input quantities using the same or similar instruments, is given by Equation (6)

$$u_c{}^2(y) = \sum_{i=1}^{N} \left(\frac{\partial f}{\partial x_\mathrm{i}}\right)^2 u^2(x_\mathrm{i}) + 2 \sum_{i=1}^{N-1} \sum_{j=i+1}^{N} \left(\frac{\partial f}{\partial x_\mathrm{i}}\right)\left(\frac{\partial f}{\partial x_\mathrm{j}}\right) u(x_\mathrm{i}, x_\mathrm{j}) \tag{6}$$

where x_i and x_j are the estimates of X_i and X_j and $u(x_\mathrm{i}, x_\mathrm{j}) = u(x_\mathrm{j}, x_\mathrm{i})$ is the estimated covariance associated with x_i and x_j. The degree of linear correlation between x_i and x_j is characterized by the estimated correlation coefficient, shown in Equation (7)

$$r(x_\mathrm{i}, x_\mathrm{j}) = \frac{u(x_\mathrm{i}, x_\mathrm{j})}{u(x_\mathrm{i})\, u(x_\mathrm{j})} \tag{7}$$

where $r(x_\mathrm{i}, x_\mathrm{j}) = r(x_\mathrm{j}, x_\mathrm{i})$, and $-1 \le r(x_\mathrm{i}, x_\mathrm{j}) \le +1$. Rewriting Equation (6) as a function of the correlation and sensitivity coefficients gives:

$$u_c{}^2(y) = \sum_{i=1}^{N} c_i{}^2\, u^2(x_\mathrm{i}) + 2 \sum_{i=1}^{N-1} \sum_{j=i+1}^{N} c_i\, c_j\, u(x_\mathrm{i})\, u(x_\mathrm{j})\, r(x_\mathrm{i}, x_\mathrm{j}) \tag{8}$$

equation that can be expressed in compact matrix format as

$$u_c{}^2(y) = \boldsymbol{g}^T \boldsymbol{cov}(x_i)\, \boldsymbol{g} \tag{9}$$

where the covariance matrix $\boldsymbol{cov}(\boldsymbol{x_i})$ is defined as:

$$\boldsymbol{cov}(x_i) = \begin{bmatrix} u^2(x_1) & r(x_1, x_2)\, u(x_1)\, u(x_2) & \dots & r(x_1, x_n)\, u(x_1)\, u(x_n) \\ r(x_2, x_1)\, u(x_2)\, u(x_1) & u^2(x_2) & \dots & r(x_2, x_n)\, u(x_2)\, u(x_n) \\ \vdots & \vdots & \ddots & \vdots \\ r(x_n, x_1)\, u(x_n)\, u(x_1) & r(x_n, x_2)\, u(x_n)\, u(x_2) & \dots & u^2(x_n) \end{bmatrix} \tag{10}$$

The first-order approach delivers reasonable uncertainty estimations under the assumption that the relationship between the input quantities x_i and the measurand y is not highly nonlinear when evaluated in the expected values of the input quantities x_i and/or when the variances in measured quantities are small. One novelty of the present study is the inclusion of a second-order term in the Taylor expansion of the measurand variance $u_c(y)$, an approach previously developed by other authors as Lira [30] and Mekid and Vaja [31]. However, they considered the particular case of a single input quantity. The expression for uncertainty evaluation, considering a second-order Taylor polynomial approximation for $u_c(y)$, is given in Equation (11).

$$u_c{}^2(y) = \boldsymbol{g}^T \boldsymbol{cov}(x_i)\, \boldsymbol{g} + \frac{1}{4}\,(\boldsymbol{g}')^T \boldsymbol{krt}(x_i)\, \boldsymbol{g}' + \boldsymbol{g}^T\, \boldsymbol{skw}(x_i)\, \boldsymbol{g}' - \frac{1}{4}\,(\boldsymbol{g}')^T\, \boldsymbol{Var}^2(x_i)\, \boldsymbol{g}' \tag{11}$$

where

$$\boldsymbol{krt}(x_i) = \boldsymbol{E}\begin{bmatrix} (x_1-\bar{x}_1)^4 & (x_1-\bar{x}_1)^2(x_2-\bar{x}_2)^2 & \dots & (x_1-\bar{x}_1)^2(x_n-\bar{x}_n)^2 \\ (x_2-\bar{x}_2)^2(x_1-\bar{x}_1)^2 & (x_2-\bar{x}_2)^4 & \dots & (x_2-\bar{x}_2)^2(x_n-\bar{x}_n)^2 \\ \vdots & \vdots & \ddots & \vdots \\ (x_n-\bar{x}_n)^2(x_1-\bar{x}_1)^2 & (x_n-\bar{x}_n)^2(x_2-\bar{x}_2)^2 & \dots & (x_n-\bar{x}_n)^4 \end{bmatrix} \tag{12}$$

$$\boldsymbol{skw}(x_i) = \boldsymbol{E}\begin{bmatrix} (x_1-\bar{x}_1)^3 & (x_1-\bar{x}_1)(x_2-\bar{x}_2)^2 & \dots & (x_1-\bar{x}_1)(x_n-\bar{x}_n)^2 \\ (x_2-\bar{x}_2)(x_1-\bar{x}_1)^2 & (x_2-\bar{x}_2)^3 & \dots & (x_2-\bar{x}_2)(x_n-\bar{x}_n)^2 \\ \vdots & \vdots & \ddots & \vdots \\ (x_n-\bar{x}_n)(x_1-\bar{x}_1)^2 & (x_n-\bar{x}_n)(x_2-\bar{x}_2)^2 & \dots & (x_n-\bar{x}_n)^3 \end{bmatrix} \tag{13}$$

and

$$\boldsymbol{Var}^2(x_i) = \begin{bmatrix} u^4(x_1) & u^2(x_1)u^2(x_2) & \dots & u^2(x_1)u^2(x_n) \\ u^2(x_2)u^2(x_1) & u^4(x_2) & \dots & u^2(x_2)u^2(x_n) \\ \vdots & \vdots & \ddots & \vdots \\ u^2(x_n)u^2(x_1) & u^2(x_n)u^2(x_2) & \dots & u^4(x_n) \end{bmatrix} \tag{14}$$

It should be noted that in all the matrices above $\bar{x}_i$ denotes the mean value for the input quantity x_i.

Equation (11) introduces the vector $\boldsymbol{g}'$ defined by Equation (15)

$$\boldsymbol{g}' = \begin{bmatrix} \dfrac{\partial^2 y}{\partial {x_1}^2} & \dfrac{\partial^2 y}{\partial {x_2}^2} & \dots & \dfrac{\partial^2 y}{\partial {x_n}^2} \end{bmatrix}^{\boldsymbol{T}} \tag{15}$$

Equation (11) propagates not only the standard uncertainty $u(x_i)$ of the input quantities x_i, but also their skewness and kurtosis, the third and fourth-order moments of their probability density functions, respectively. For the sake of brevity in this presentation, the derivation of Equation (11) is left for Appendix A.

In this work, *GUM* [8] methodology is applied to quantify the uncertainty in elastomeric isolators effective properties k_{eff} and β_{eff}. To evaluate uncertainty of these properties, models relating the measurands k_{eff} and β_{eff} and their input variables are shown in Equations (16) and (17),

$$k_{eff} = \frac{|F^+| + |F^-|}{|\Delta^+| + |\Delta^-|} \tag{16}$$

$$\beta_{eff} = \frac{2}{\pi}\frac{E_{loop}}{k_{eff}(|\Delta^+| + |\Delta^-|)^2} \tag{17}$$

where F^+ and F^- are the maximum positive and minimum negative forces, measured at the cycle maximum positive and negative displacements Δ^+ and Δ^-, respectively, as shown in Figure 2(c). The energy E_{loop} is the one dissipated per loading cycle, as it is schematically shown in Figure 2(d.)
It should be emphasized that in equations (16) and (17), the absolute value operators can be removed, taking advantage of the fact that the force-displacement relationship can always be centered around the zero displacement reference. In that case, the equations can be rewritten as:

$$k_{eff} = \frac{F^+ - F^-}{\Delta^+ - \Delta^-} \tag{18}$$

$$\beta_{eff} = \frac{2}{\pi} \frac{E_{loop}}{k_{eff}(\Delta^+ - \Delta^-)^2} \tag{19}$$

To assess the uncertainty of the measurands k_{eff} and β_{eff} through Equation (9) it is necessary to calculate coefficients quantifying the sensitivity of the measurand y to variations in the input variables x_i. Given the Equations (18) and (19), the sensitivity coefficients are defined by Equations (20) – (27).

$$\frac{\partial k_{eff}}{\partial F^+} = \frac{1}{\Delta^+ - \Delta^-} \tag{20}$$

$$\frac{\partial k_{eff}}{\partial F^-} = \frac{-1}{\Delta^+ - \Delta^-} \tag{21}$$

$$\frac{\partial k_{eff}}{\partial \Delta^+} = \frac{-(\mathrm{F}^+ - \mathrm{F}^-)}{(\Delta^+ - \Delta^-)^2} \tag{22}$$

$$\frac{\partial k_{eff}}{\partial \Delta^-} = \frac{\mathrm{F}^+ - \mathrm{F}^-}{(\Delta^+ - \Delta^-)^2} \tag{23}$$

$$\frac{\partial \beta_{eff}}{\partial E_{loop}} = \frac{2}{\pi\, k_{eff}(\Delta^+ - \Delta^-)^2} \tag{24}$$

$$\frac{\partial \beta_{eff}}{\partial k_{eff}} = -\frac{2}{\pi} \frac{E_{loop}}{{k_{eff}}^2(\Delta^+ - \Delta^-)^2} \tag{25}$$

$$\frac{\partial \beta_{eff}}{\partial \Delta^+} = -\frac{4}{\pi} \frac{E_{loop}}{k_{eff}(\Delta^+ - \Delta^-)^3} \tag{26}$$

$$\frac{\partial \beta_{eff}}{\partial \Delta^-} = \frac{4}{\pi} \frac{E_{loop}}{k_{eff}(\Delta^+ - \Delta^-)^3} \tag{27}$$

For the second-order Taylor approximation implemented in this study, the second derivatives of the measurands y_i (i.e., k_{eff} and β_{eff}) with respect to the input quantities x_i (F^+, F^-, Δ^+, Δ^-,k_{eff}, and E_{loop}) are required to evaluate the $\boldsymbol{g'}$ matrix. Given the lengthy derivations, these expressions are presented in Appendix B.

2.3 Identifying uncertainty sources for input quantities x_i

As Equations (18) and (19) show, measurands k_{eff} and β_{eff} depend on four input quantities, namely F^+, F^-, Δ^+, and Δ^-, since the two additional quantities E_{loop} and k_{eff}, could be considered intermediate quantities in the calculation of β_{eff}, as their expected values and standard uncertainties also depend on force and displacement measurements.
The definition of k_{eff} is given by equation (18) and E_{loop} is defined in equation (28)

$$\left(E_{loop}\right)_j = \sum_{i=1}^{p-1} \frac{1}{2}\left((F_i)_j + (F_{i+1})_j\right)\Delta_{int} \tag{28}$$

where F_{i} with i ranging from 1 to p are consecutive force measurements at a given displacement increment Δ_{int}, defining the complete measured-by-test force-displacement curve.

Hence, the sources of uncertainty for the input quantities F^+, F^-, Δ^+, Δ^-, and F_{i} need to be studied. A certain degree of correlation is expected between the force-related input quantities (i.e., F^+, F^-, and F_{i}) and between the displacement-related input quantities (i.e., Δ^+ and Δ^-) since they are measured using the same instrumental setup, same instrument, and instrument's same location. This degree of correlation increases as the force-displacement curves are centered around the zero-displacement reference, implying that Δ^+ and Δ^- have the same absolute value, and F^+ and F^- present only slight differences between their absolutes values, given the symmetry of the curves. Therefore, uncertainty quantification needs to be performed using Equations (9) and (11) for correlated input quantities.

2.3.1 Uncertainty sources for force measurement

The uncertainty sources for force measurement considered in this work are: (i) Type-A uncertainty arising from different measurements performed under *repeatability conditions*; (ii) Type-B uncertainty obtained from measurement tolerance of the force transducer (load-cell); (iii) Type-B uncertainty obtained from a calibration certificate; and (iv) Type-B uncertainty inherent to the measurement instrument resolution.

2.3.2 Uncertainty sources for displacement measurement

The uncertainty sources for displacement measurement considered in this work are: (i) Type-A uncertainty arising from different measurements performed under *repeatability conditions*; (ii) Type-B uncertainty obtained from measurement tolerance of the linear variable differential transducer (LVDT), (iii) Type-B uncertainty obtained from the calibration certificate; and (iv) Type-B uncertainty inherent to measurement instrument resolution.

Figures 3 and 4 show the Ishikawa diagrams (cause-effect diagrams) with the considered uncertainties for k_{eff} and β_{eff} uncertainty assessment.

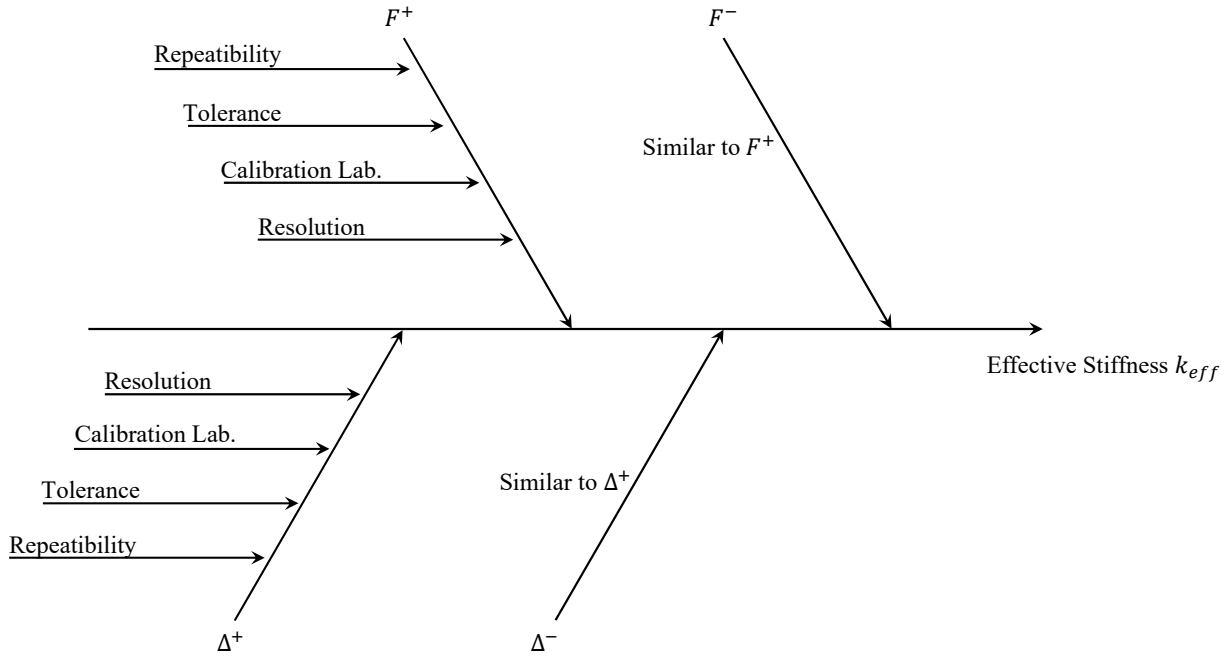

Figure 3. Ishikawa Diagram for effective stiffness uncertainty quantification

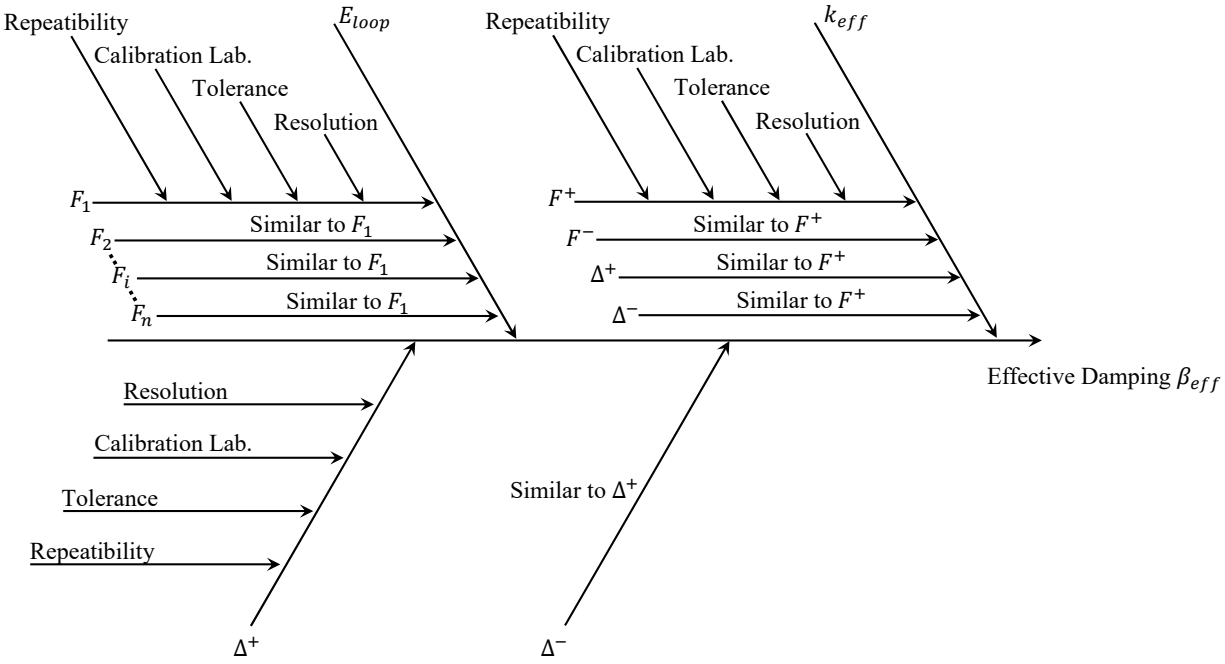

Figure 4. Ishikawa Diagram for damping ratio uncertainty quantification

2.4 Monte-Carlo simulation methodology

As GUM Supplement 1 [10] states, any method used to estimate uncertainty should include the stages of formulation, propagation, and summarizing. Once the probability distributions of the input quantities are defined, they need to be propagated to the output quantity, i.e., the measurand. Monte-Carlo method (MCM in *GUM* terminology) performs this propagation numerically by performing random sampling from probability distributions of the input quantities. The following steps were implemented in this work:

1. The number of trials *M* was defined. In this case, a maximum of 2,000,000 trials was used. Because this simulation does not require a high amount of computational time, the adaptive Monte-Carlo method was not implemented. A sensitivity analysis studying the influence of the number of trials *M* on the quantified uncertainty was performed.
2. *M* realizations of the set of *N* input quantities were generated. As stated in [10], a Gaussian probability distribution function was assigned to each input quantity with a mean equal to the quantity estimate and a standard deviation equal to the associated combined standard uncertainty. For example, for Specimen 1, the means and standard deviations are shown in Tables (2),(3),(5), and (7).
   Two different calculation scenarios were studied, considering uncorrelated and correlated input quantities. In the latter case, the correlation coefficients (for the particular case of Specimen 1) are reported in tables (4) and (6).
3. For each realization, the value of the measurand *Y* was calculated using the corresponding model equation.
4. The *M* generated values of the measurand *Y* were sorted to approximate the probability density function **G** of the measurand.
5. An estimation of the measurand *y*, its standard uncertainty *u(y),* and an appropriate coverage interval can be calculated from the probability density function **G.**

3. Uncertainty Quantification – Results

The *GUM* methodology was applied to assess the uncertainty of the effective properties of all isolators in the dataset. Histograms for the expanded relative uncertainty (i.e., the ratio of property expanded uncertainty to property mean value) are shown in Figures 5 through 8. To elucidate the methodology, Tables 2 to 5 show the uncertainty budget and the uncertainty quantification for the effective stiffness k_{eff} and the effective damping β_{eff} for a specific isolator hereafter referred to as Specimen 1 with an external diameter $D_{ext} = 70\ cm$, an internal diameter $D_{int} = 10\ cm$, and

a total rubber height $H_r = 16.2\ cm$. As effective stiffness k_{eff} is calculated using Equation (18), the uncertainty sources for the input quantities F^+, F^-, Δ^+, and Δ^- need to be investigated. Results are only reported for shear deformation $\gamma = 1.5$, but similar trends are observed with other levels of shear deformations.

3.1 Specimen 1 uncertainties – *GUM* Method

3.1.1 Uncertainty sources for force measurements $F^+$and F^-

Uncertainty arising from several measurements under repeatability conditions

The uncertainty arising from several measurements under *repeatability conditions* is evaluated as the sample standard deviation of the mean value with the expression:

$$u(F^+_{rep}) = \sqrt{\frac{\sum_{j=1}^{n}(F^+_j - \overline{F^+})^2}{\frac{n-1}{n}}}$$
$$u(F^-_{rep}) = \sqrt{\frac{\sum_{j=1}^{n}(F^-_j - \overline{F^-})^2}{\frac{n-1}{n}}} \quad (29)$$

where F^+_j is the force value associated with the maximum displacement for testing cycle j; $\overline{F^+}$ is the mean value of the forces associated with the maximum displacements for all cycles; and n is the number of cycles considered in the analysis, i.e., five cycles ranging from first to fifth or from second to sixth. As the measurand expected value is calculated by evaluating the model equation in the mean values of the input quantities, the standard deviation of the mean of the input quantity shall be used [30]. The uncertainty for F^- is calculated following an analogous procedure.

Uncertainty arising from the force measuring device and its calibration tolerance

As stated in the calibration report [32], the maximum acceptable deviation specified for the load cell is defined as 1% of the peak applied force value. Nevertheless, a more realistic uncertainty value of the maximum deviation effectively observed during the calibration procedure was assigned to F^+ and F^-. This value was 0.64% of the measured value. Giving that $\overline{F^+}$ and $\overline{F^-}$ for the analyzed specimen are 235.8594 kN and -236.1563 kN, the standard uncertainty values are 1.5095 kN and 1.5114 kN, for $\overline{F^+}$ and $\overline{F^-}$, respectively.

Uncertainty arising from calibration laboratory uncertainty

As stated in [32], the MTS calibration laboratory force measurement expanded uncertainty (U) is 0.34% of the applied force. This value was calculated using and coverage factor (k) of 2.0 for an estimated level of confidence of 95%. Given that coverage factor, the standard uncertainty is given by the expression:

$$u(F^+_{cal}) = \frac{U}{k} = \frac{0.34\%}{2} = 0.17\ \% \quad (30)$$

resulting in a force uncertainty of 0.17% for the measured mean value of $\overline{F^+}$ and $\overline{F^-}$.

Uncertainty arising from measurement instrument resolution

As stated in [32], the force measuring resolution is 0.002 kN. Given a uniform probability distribution function in the resolution interval, the standard uncertainty due to resolution is given by the expression

$$u(F^+_{res}) = \frac{0.002\ kN}{2\sqrt{3}} = 0.0012\ kN \quad (31)$$

As all sources of variability described above are assumed independent and mutually uncorrelated, it can be stated that:

$$\boldsymbol{u^2(F^+)} = u^2({F^+}_{rep}) + u^2({F^+}_{tol}) + u^2({F^+}_{cal}) + u^2({F^+}_{res}) \quad (32)$$

$$\boldsymbol{u^2(F^-)} = u^2({F^-}_{rep}) + u^2({F^-}_{tol}) + u^2({F^-}_{cal}) + u^2({F^-}_{res}) \quad (33)$$

The different uncertainty sources for F^+ and F^- and their corresponding values are summarized in Table 2

Table 2 Summary of standard uncertainty components for F^+ and F^-

Standard uncertainty component $u(x_i)$	Source of uncertainty	Distribution type	Value of standard uncertainty $u(x_i)$
$\boldsymbol{u(F^+)}$			**2.6583 kN**
${u(F^+}_{rep})$	Repeatability	Normal	2.1511 kN
${u(F^+}_{tol})$	Tolerance	Normal	1.5095 kN
${u(F^+}_{cal})$	Calibration	Normal	0.4009 kN
${u(F^+}_{res})$	Resolution	Uniform	5.7735e-04 kN
$\boldsymbol{u(F^-)}$			**2.6901 kN**
${u(F^-}_{rep})$	Repeatability	Normal	2.1888 kN
${u(F^-}_{tol})$	Tolerance	Normal	1.5114 kN
${u(F^-}_{cal})$	Calibration	Normal	0.4015 kN
${u(F^-}_{res})$	Resolution	Uniform	5.7735e-04 kN

3.1.2 Uncertainty sources for displacement measurements Δ^+ and Δ^-

Uncertainty arising from several measurements under repeatability conditions

The uncertainty arising from several displacement measurements under *repeatability conditions* is evaluated as the sample standard deviation of the mean value with the expression:

$$u\left({\Delta^+}_{rep}\right) = \sqrt{\frac{\sum_{j=1}^{n}({\Delta^+}_j - \overline{\Delta^+})^2}{\frac{n-1}{n}}}$$

$$u\left({\Delta^-}_{rep}\right) = \sqrt{\frac{\sum_{j=1}^{n}({\Delta^-}_j - \overline{\Delta^-})^2}{\frac{n-1}{n}}} \quad (34)$$

where ${\Delta^+}_j$ is the maximum displacement for testing cycle *j*; $\overline{\Delta^+}$ is the mean value of the maximum displacements for all cycles; and n is the number of cycles. All assumptions used in the uncertainty evaluation of the forces were also applied for displacements.

Uncertainty arising from the displacement measuring transducer tolerance

As stated in the calibration report [33], the maximum acceptable deviation in the LVDT reading is 1% of the full-scale range. Since the full-scale range is 500 mm, the allowable deviation is 5 mm. Nonetheless, to assess a more realistic uncertainty value, the maximum deviation effectively observed during the calibration procedure was assigned to the Δ^+ and Δ^- values. This number was 0.79% of the measured value. The averages $\overline{\Delta^+}$ and $\overline{\Delta^-}$ for the analyzed specimen are 24.2453 cm and -24.2453 cm, respectively, then the standard uncertainty is 0.1915 cm for both cases.

Uncertainty arising from calibration laboratory uncertainty

As stated in [33], the uncertainty of the supplied calibration data is equal or smaller than the greater of 0.25% of the reading or 50μ inches. In this case, the former value is at least one order of magnitude larger than the latter; thus, it was selected for the uncertainty assessment. As informed in the calibration report, this value considers a coverage

factor (k) of 2.0 for an estimated level of confidence of 95%. Given that coverage factor, the standard uncertainty is given by the expression:

$$u(\Delta^+{}_{cal}) = \frac{U}{k} = \frac{0.25\%}{2} = 0.125\% \tag{35}$$

resulting in a displacement uncertainty of 0.125% of the measured mean value of $\overline{\Delta^+}$ and $\overline{\Delta^-}$.

Uncertainty arising from measurement instrument resolution

As stated in [33], the displacement measurement resolution is 0.001 mm. Assuming a uniform probability distribution function for the resolution interval, the standard uncertainty due to resolution is given by the expression:

$$u(\Delta^+{}_{res}) = \frac{0.0001\ cm}{2\sqrt{3}} = 2.8868 \cdot 10^{-5}\ cm \tag{36}$$

As all the variability sources described above are independent and mutually uncorrelated, the combined standard uncertainty may be written as:

$$\boldsymbol{u^2}(\Delta^+) = u^2(\Delta^+{}_{rep}) + u^2(\Delta^+{}_{tol}) + u^2(\Delta^+{}_{cal}) + u^2(\Delta^+{}_{res}) \tag{37}$$

$$\boldsymbol{u^2}(\Delta^-) = u^2(\Delta^-{}_{rep}) + u^2(\Delta^-{}_{tol}) + u^2(\Delta^-{}_{cal}) + u^2(\Delta^-{}_{res}) \tag{38}$$

The different uncertainty sources for Δ^+ and Δ^- and their corresponding values are summarized in Table 3

Table 3 Summary of standard uncertainty components for Δ^+ and Δ^-

Standard uncertainty component $u(x_i)$	Source of uncertainty	Distribution type	Value of standard uncertainty $u(x_i)$
$\boldsymbol{u}(\Delta^+)$			**0.1939 cm**
$u(\Delta^+{}_{rep})$	Repeatability	Normal	0.0013 cm
$u(\Delta^+{}_{tol})$	Tolerance	Normal	0.1915 cm
$u(\Delta^+{}_{cal})$	Calibration	Normal	0.0303 cm
$u(\Delta^+{}_{res})$	Resolution	Uniform	2.8868e-05 cm
$\boldsymbol{u}(\Delta^-)$			**0.1939 cm**
$u(\Delta^-{}_{rep})$	Repeatability	Normal	0.0013 cm
$u(\Delta^-{}_{tol})$	Tolerance	Normal	0.1915 cm
$u(\Delta^-{}_{cal})$	Calibration	Normal	0.0303 cm
$u(\Delta^-{}_{res})$	Resolution	Uniform	2.8868e-05 cm

3.1.3 Uncertainty assessment for k_{eff}

The propagation of the standard uncertainties of F^+, F^-, Δ^+ and Δ^- to the uncertainty in the effective stiffness k_{eff} was carried out. Sensitivity coefficients in equations (20) – (23) are evaluated in the mean values of the input quantities and shown in the fourth column of Table 5. As the force input variables (F^+ and F^-) and the displacement input variables (Δ^+ and Δ^-) are recorded with the same measuring devices, and both objective displacements have the same absolute value; the correlation between these input quantities needs to be considered in the calculation. The correlation coefficients for the input variables F^+, F^-, Δ^+ and Δ^- are shown in Table 4:

Table 4 Correlation coefficients between input quantities F^+, F^-, Δ^+ and Δ^-

	F^+	F^-	Δ^+	Δ^-
F^+	1	-0.9253	-0.3278	0.3278
F^-	-0.9253	1	0.5650	-0.5650
Δ^+	-0.3278	0.5650	1	-1
Δ^-	0.3278	-0.5650	-1	1

Finally, evaluating equation (8), or its matrix equivalent equation (9), the expanded uncertainty for the measurand k_{eff} is 0.3433 kN/cm. As the expected value of the measurand is 9.7342 kN/cm, the relative expanded uncertainty is 3.53%. For assessing the coverage factor, that applied over the standard uncertainty results in the expanded uncertainty; the well-known Welch-Satterthwaite formula was used, implementing the version adapted for correlated input quantities [30,34]. The number of effective degrees of freedom was 14.4 and $t_{95} = 2.14$.

Table 5 Summary of standard uncertainty components for k_{eff}

Standard uncertainty component $u(x_i)$	Expected value $\bar{x}_i$	Value of standard uncertainty $u(x_i)$	$c_i = \partial k_{eff}/\partial x_i$ (evaluated at $\bar{x}_i$)	Value of combined expanded uncertainty $u(\boldsymbol{k_{eff}})$	Value of relative expanded uncertainty %
$\boldsymbol{u(k_{eff})}$	**9.7342 kN/cm**			**0.3433 kN/cm**	**3.53 %**
$u(F^+)$	235.8518 kN	2.6583 kN	0.0206 1/cm		
$u(F^-)$	-236.1639 kN	2.6901 kN	-0.0206 1/cm		
$u(\Delta^+)$	24.2453 cm	0.1939 cm	-0.2007 kN/cm^2		
$u(\Delta^-)$	-24.2453 cm	0.1939 cm	0.2007 kN/cm^2		

It is interesting to note the signs of the 4th column terms. Since they represent $\partial k_{eff}/\partial x_i$, for F^+ the sensitivity of k_{eff} must be positive since an increase in F^+ produces an increase in k_{eff}. The opposite occurs for F^- given its algebraic sign. On the other hand, for $\partial k_{eff}/\partial \Delta^+$, an increase in Δ^+ produces a decrease in k_{eff} at this level of deformation (24.2453 cm), and the opposite occurs for Δ^-. Moreover, the uncertainty of k_{eff} was calculated with Equation (11) to include the second-order term in the Taylor polynomial approximation. However, there was no significant difference in the uncertainty value when the second-order terms were included, since in this case, they are at least four orders of magnitude smaller than the first-order terms.

3.1.4 Uncertainty assessment for β_{eff}

The uncertainty in the effective damping β_{eff} was also calculated. As can be seen in Equation (19), the assessment of the uncertainty of β_{eff} requires as an intermediate step the uncertainty quantification of k_{eff} and E_{loop}.

The uncertainty quantification of k_{eff} was presented in the previous section, but the assessment of the uncertainty of E_{loop} requires a different methodology, as E_{loop} corresponds to the area enclosed by the force-displacement curve in a full deformation cycle, as defined above in equation (28). The proposed method resamples the displacement values of the force-displacement curve at a new displacement interval, say $\Delta_{int} = 0.1\ cm$. Once the displacements are resampled, a new set of input forces $F_1, F_2, F_3, \dots, F_p$, where p is the number of points defining the resampled curve, need to be considered. For each one of these new input quantities, there are as many measured values of force F_i as cycles were carried out during the test. Then, the uncertainty of E_{loop} was evaluated using the equation (28) model to integrate the force-displacement relationship for cycle j using the trapezoidal rule. As it was explained in the previous section, the correlation between the input quantities E_{loop}, k_{eff}, Δ^+ and Δ^- needs to be considered in the uncertainty quantification of β_{eff}. The correlation coefficients used in the calculation are shown in Table 6.

Finally, evaluating equation (8)-(9), the expanded uncertainty for the measurand β_{eff} is 0.0045. Given that the expected value of β_{eff} is 0.1239, the relative expanded uncertainty is 3.61 %. In this case, the number of effective degrees of freedom was 8.4, and $t_{95} = 2.31$.

Table 6 Correlation coefficients between input variables E_{loop}, k_{eff}, Δ^+ and Δ^-

	E_{loop}	k_{eff}	Δ^+	Δ^-
E_{loop}	1	0.989	-0.5648	0.5648
k_{eff}	0.989	1	-0.457	0.457
Δ^+	-0.5648	-0.457	1	-1
Δ^-	0.5648	0.457	-1	1

Table 7 Summary of standard uncertainty components for β_{eff}

Standard uncertainty component $u(x_i)$	Expected value $\bar{x}_i$	Value of standard uncertainty $u(x_i)$	$c_i = \partial\beta_{eff}/\partial x_i$ (evaluated at $\bar{x}_i$)	Value of combined expanded uncertainty $u(\boldsymbol{\beta_{eff}})$	Value of relative expanded uncertainty %
$\boldsymbol{u(\beta_{eff})}$	**0.1239**			**0.0045**	**3.61 %**
$u(E_{loop})$	4.4538e03 kN cm	17.1108 kN cm	2.781e-5 1/kN cm		
$u(k_{eff})$	9.7342 kN	0.1600 kN/cm	-0.0127 cm/kN		
$u(\Delta^+)$	24.2453 cm	0.1939 cm	-0.0051 1/cm		
$u(\Delta^-)$	-24.2453 cm	0.1939 cm	0.0051 1/cm		

The expanded uncertainty was also evaluated using the second-order Taylor approximation for the variance of β_{eff}, as defined in Equation (11). A slight difference of 1% between the second-order and the first-order approximation was observed in this particular case.

3.2 Specimen 1 uncertainties – Comparison between *GUM* and Monte-Carlo results.

As stated previously in section 2.4 and looking to quantify the relevance of the correlation among the input quantities in these uncertainty assessments, the Monte-Carlo simulations were performed under two scenarios. In the first case, the correlation between the input quantities was considered, and in the second case, the input quantities were considered uncorrelated. Tables 8 and 9 show the percentual difference between the uncertainty assessed using Monte-Carlo simulation and the *GUM* methodology, defined as $(MCM - GUM)/GUM$. Additionally, to study the results' stability, the Monte-Carlo simulations were performed using different numbers of trials *M*.

Table 8 Percentual difference between *GUM* and Monte-Carlo estimation of uncertainty of k_{eff}, Specimen 1

Shear Strain	MCM with correlated input quantities				MCM with uncorrelated input quantities			
	M=2,000	*M* =20,000	*M* =200,000	*M* =2,000,000	*M* =2,000	*M* =20,000	*M* =200,000	*M* =2,000,000
0.25	-0.73%	0.22%	0.10%	0.08%	14.57%	17.46%	16.83%	17.09%
0.50	0.32%	-0.48%	0.14%	0.03%	-24.87%	-22.87%	-22.29%	-22.45%
1.00	3.34%	0.23%	0.07%	-0.10%	-25.75%	-25.17%	-26.41%	-25.97%
1.50	-1.10%	0.28%	0.11%	-0.12%	-30.33%	-28.39%	-28.59%	-28.54%

Table 9 Percentual difference between *GUM* and Monte-Carlo estimation of uncertainty of β_{eff}, Specimen 1

Shear Strain	MCM with correlated input quantities				MCM with uncorrelated input quantities			
	M=2,000	*M* =20,000	*M* =200,000	*M* =2,000,000	*M* =2,000	*M* =20,000	*M* =200,000	*M* =2,000,000
0.25	1.04%	-1.57%	0.23%	0.19%	14.13%	16.65%	16.32%	16.75%
0.50	-0.06%	0.83%	0.70%	0.76%	22.56%	17.46%	19.40%	19.34%
1.00	-0.65%	0.53%	-0.45%	-0.37%	37.75%	30.12%	30.69%	30.90%
1.50	1.98%	-0.59%	0.36%	0.31%	89.40%	93.69%	93.49%	93.57%

As it was explained in the previous sections, when the effective properties' uncertainties are assessed, the correlation among the input quantities needs to be considered. Based on that fact, when the correlated MCM results are compared with the ones obtained with *GUM*, the percentual differences are noticeably small for all cases under analysis, being

the maximum differences 3.34% and 1.98% for stiffness and damping, respectively. It should be noticed that these differences are associated with simulations performed using a small number of realizations (M = 2,000). As the number of realizations increases (M = 200,000) these percentual differences decrease, not surpassing 1.00% in any case under analysis. It is interesting to study the effect of the correlations in the uncertainty assessments. In the calculation of the uncertainties in the effective stiffness k_{eff}, the uncorrelated uncertainties are smaller than the correlated (and correct) ones, presenting differences ranging from 22% to 29% for shear strains higher than $\gamma = 0.5$. On the other hand, the effective damping β_{eff} uncertainties, calculated using uncorrelated input quantities, are consistently higher than the correlated (and correct) ones, with differences ranging from 17% to 94%.

3.3 Dataset uncertainty results

Figures (5) and (6) show histograms of the expanded relative uncertainties associated with the k_{eff} and β_{eff} estimates of the 2,498 seismic isolators, respectively. Only one Type-A uncertainty source was considered (several measurements under *repeatability conditions*). As prescribed in NCh 2745 [2], properties and uncertainties were evaluated considering deformation cycles 2 through 6, being these histograms displayed in subplots (a) and (b) for the four shear deformations considered. For comparison purposes, properties and uncertainties were also evaluated considering cycles 1 through 5, being these results displayed in subplots (c) and (d).

The selection of the cycles to generate the averages has a predictable consequence in the uncertainty of the effective stiffness k_{eff} since, the mean uncertainties for the *unscragged or virgin* case (averaging cycles 1 through 5) are higher than the ones for the *scragged* or *stable* case (cycles 2 through 6). For the sake of clarity, the *unscragged or virgin* case is the one where the softening has not been developed, and the *scragged* or *stable* case is the one where the softening has been fully developed [35]. When comparing standard deviations of the uncertainty, a clear trend is noticed as they are consistently higher in the *unscragged* case, with ratios ranging from 1.40 to 1.94 times relative to the *scragged* case. Furthermore, on average, the mean uncertainties observed for Compound 1 are slightly but consistently higher than the ones for Compound 2. As some of the figures show, the histograms are not necessarily symmetric. Some histograms are skewed, implying that the calculated uncertainties do not necessarily follow a normal distribution. This fact could be anticipated since most of the dataset uncertainty values are small but, by definition, positive, constraining the histogram's shape and making it depart from the characteristical shape of a Gaussian distribution. The relevant statistics of the uncertainties' full dataset are reported in Tables (10) and (11).

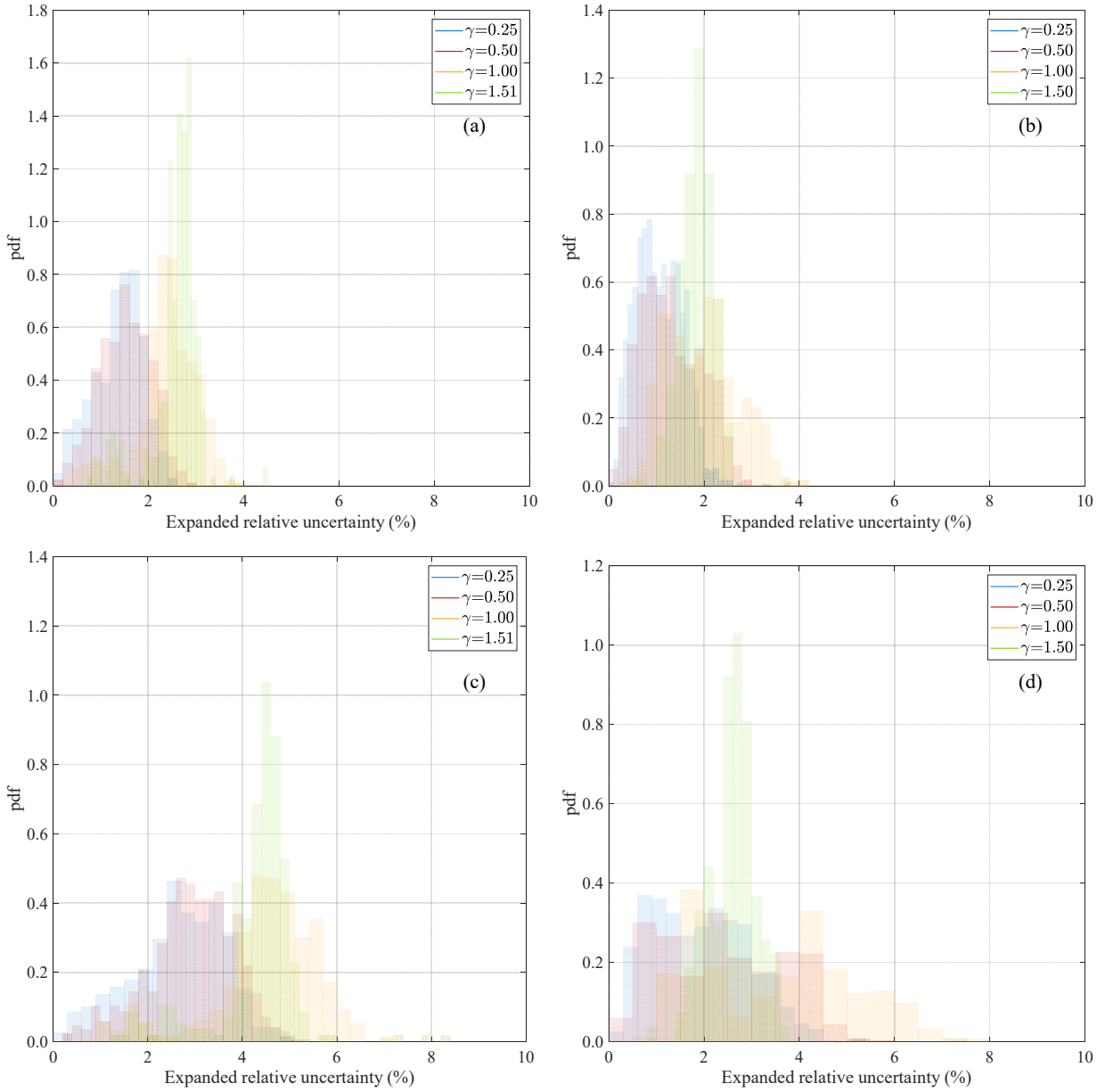

Figure 5. Expanded relative uncertainty in equivalent stiffness k_{eff} for the seismic isolators dataset, considering only intercycle uncertainty: (a) Compound 1, using cycles 2 through 6, (b) Compound 2, using cycles 2 through 6, (c) Compound 1, using cycles 1 through 5, and (d) Compound 2, using cycles 1 through 5

Figure 6 shows data histograms for the expanded relative uncertainty of β_{eff}. Just as it was observed for k_{eff}, the mean uncertainties for Compound 1 are mildly but consistently higher than the mean uncertainties for Compound 2. Nevertheless, there are no consistent trends between the means of the *scragged* and *unscragged* cases. Uncertainty assessment of effective damping β_{eff} involves measured values from the whole force-displacement curve, thus reducing the *scragging* relevance, since the *scragged* and *unscragged* curves are similar for low levels of lateral deformation. Additionally, as the E_{loop} term involves the summation of small areas in each displacement increment, a smoothing effect appears as the calculation is less sensitive to the differences of the forces in each cycle. On the other hand, uncertainty assessment of the effective stiffness k_{eff} only considers the extreme values of the curves, thus leading to much more noticeable differences between the *scragged* and *unscragged* curves.

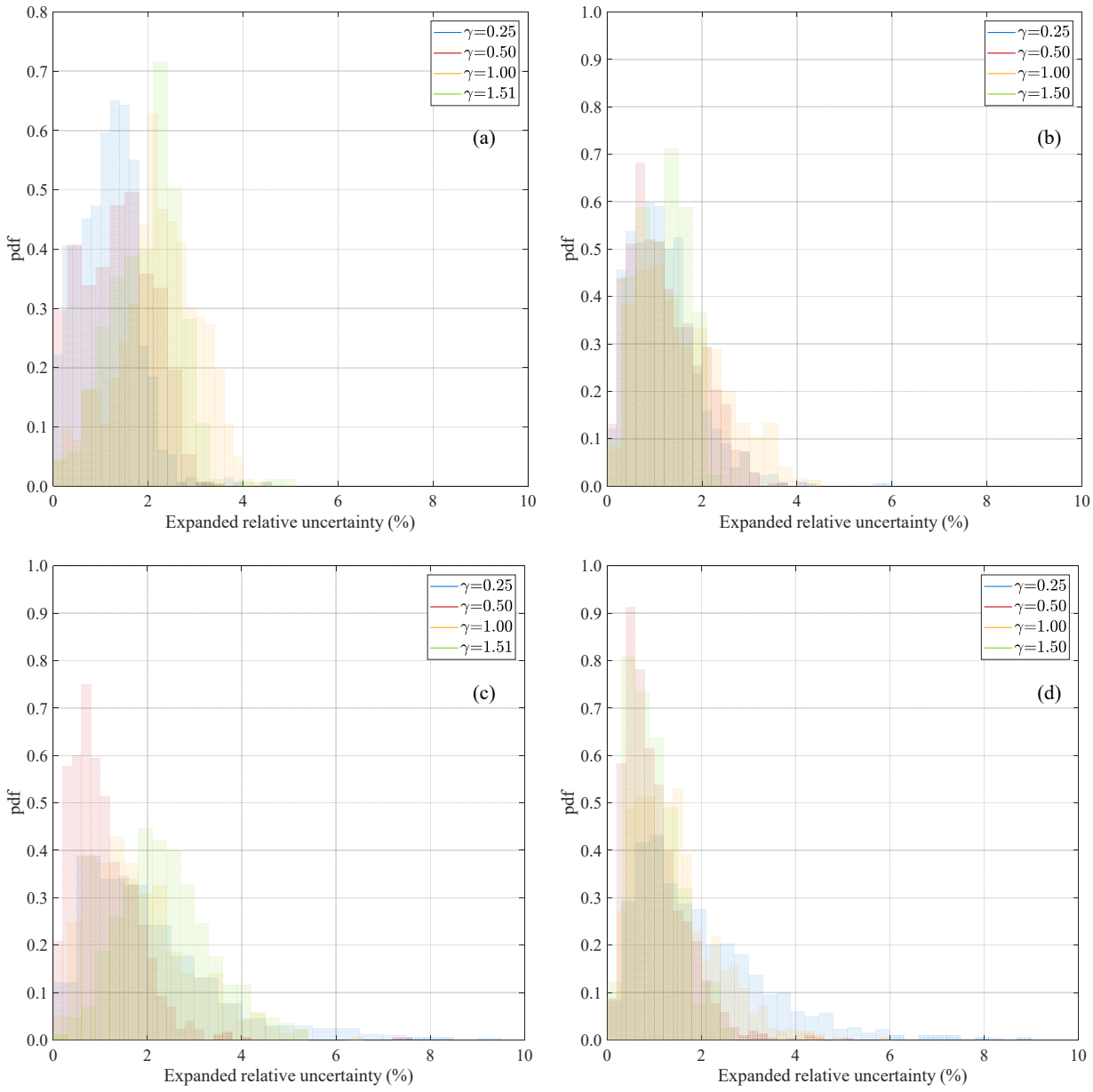

Figure 6. Expanded relative uncertainty for the effective damping β_{eff} of the seismic isolator dataset, considering only intercycle uncertainty: (a) cycles 2 to 6 of Compound 1, (b) cycles 2 to 6 of Compound 2, (c) cycles 1 to 5 of Compound 1, and (d) cycles 1 to 5 of Compound 2

Figures (7) and (8) show histograms analogous to the ones presented in Figures (5) and (6), but considering Type-B uncertainty sources of tolerance, calibration, and resolution, as detailed in the example specimen, in addition to the variability under *repeatability conditions* (uncertainty source Type-A).

Results from uncertainties in effective stiffness k_{eff} are shown in Figure 7. *Unscragged* mean uncertainties surpass their *scragged* counterpart values with ratios ranging from 1.32 to 1.82, and from 1.15 to 1.68, for Compounds 1 and 2, respectively. These ratios can be predicted as linear functions of shear strain γ, for values of γ ranging from 0.25 to 1.0. Standard deviations of the uncertainty are consistently higher for the *unscragged* case.

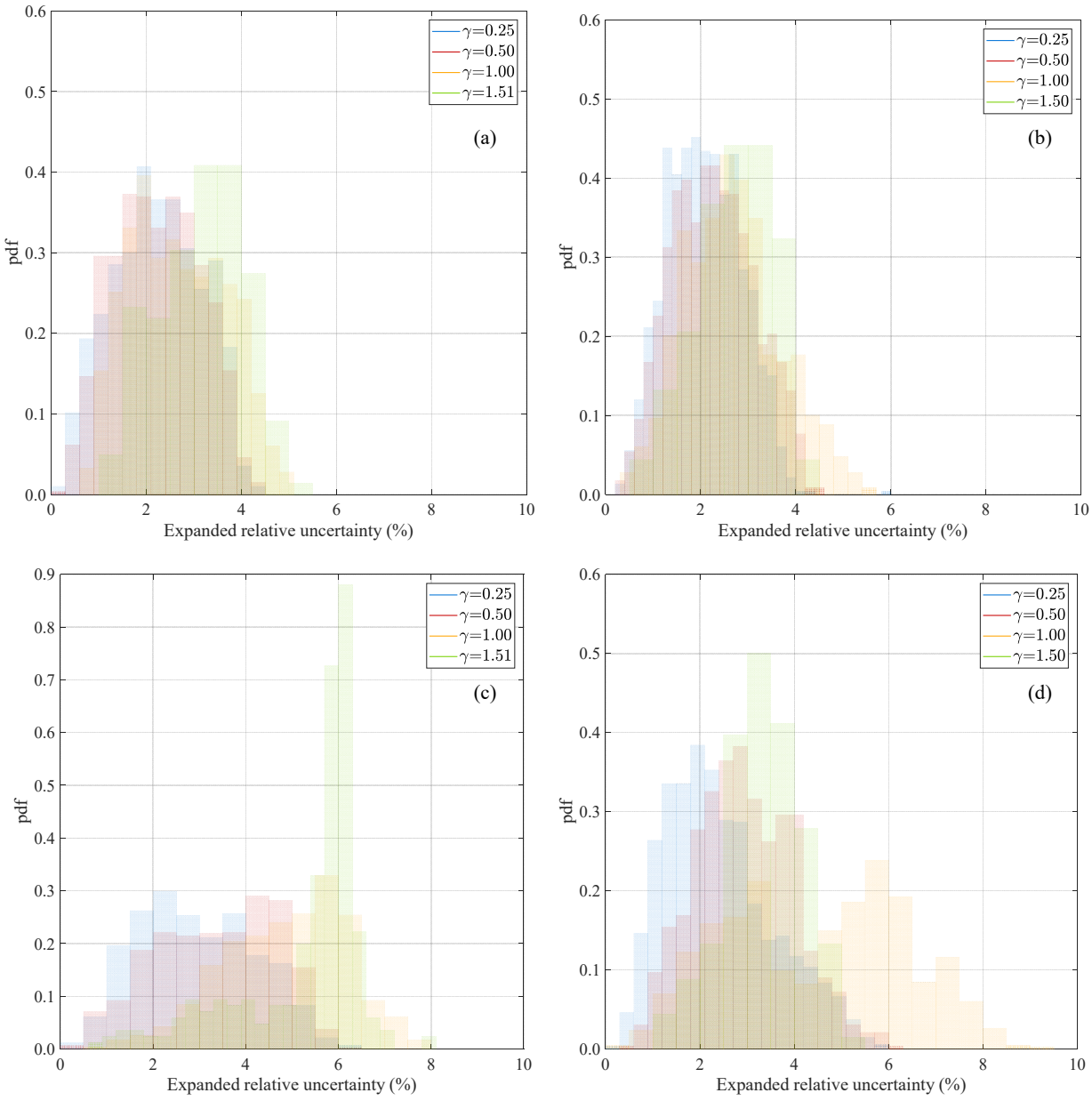

Figure 7. Expanded relative uncertainty in equivalent stiffness k_{eff} for the seismic isolators dataset, considering intercycle uncertainty and Type B uncertainty sources: (a) compound 1, using cycles 2 through 6, (b) compound 2, using cycles 2 through 6, (c) compound 1, using cycles 1 through 5, and (d) compound 2, using cycles 1 through 5

Results of Figure 8 present the effective damping β_{eff} and do not show a clear trend between mean uncertainties for the *scragged* and *unscragged* cases. Probability density functions look similar for all the cases under analysis, showing that uncertainty in β_{eff} is less sensitive to differences in Compounds, shear strains, or cycle selection than uncertainty in k_{eff}.

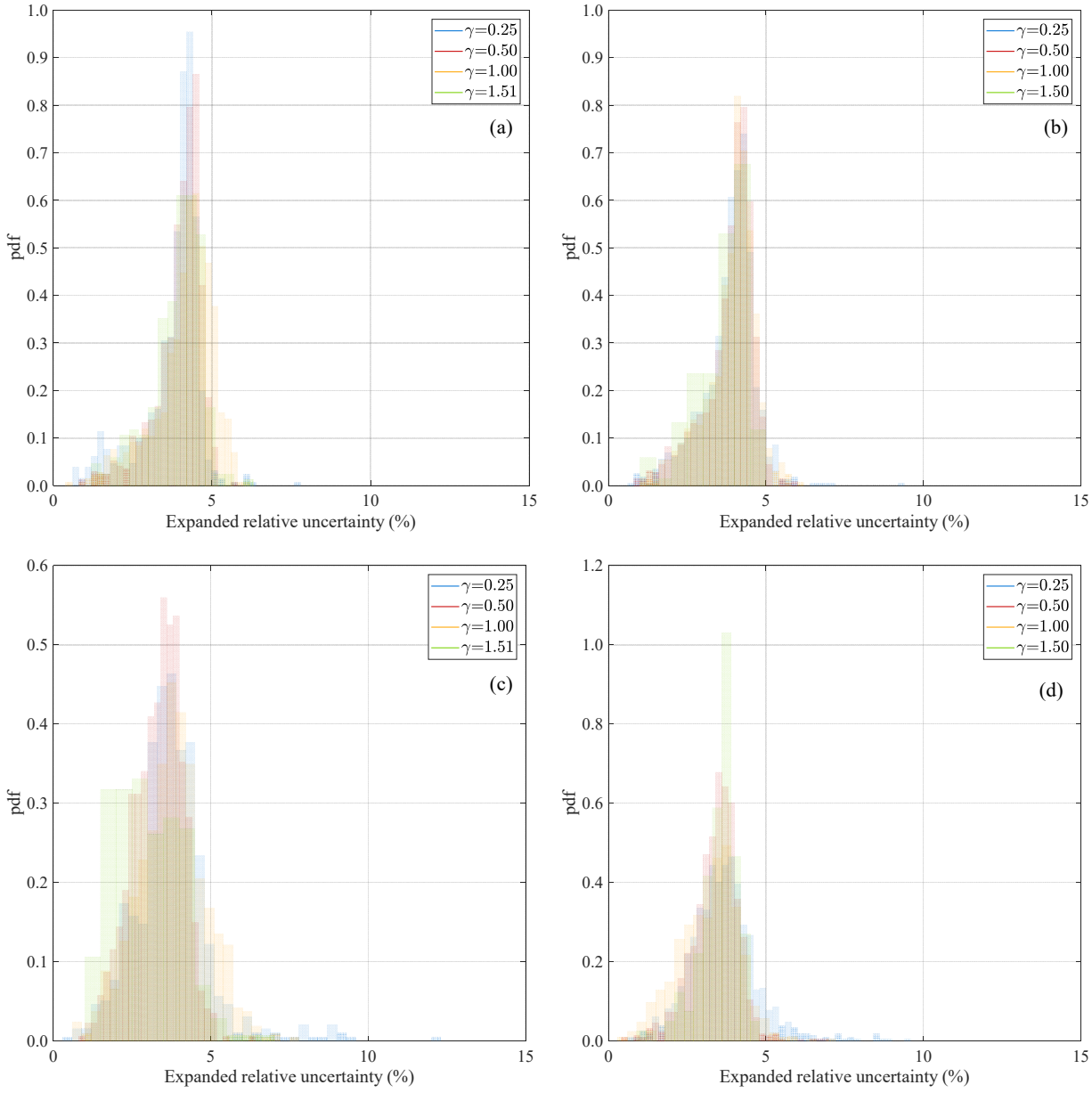

Figure 8. Expanded relative uncertainty of the equivalent damping ratio β_{eff} for the seismic isolators dataset, considering intercycle uncertainty and Type B uncertainty sources: (a) Cycles 2 through 6 of Compound 1, (b) Cycles 2 through 6 of Compound 2, (c) Cycles 1 through 5 of Compound 1, and (d) Cycles 2 through 5 of Compound 2

It could be stated that observations from data in Figures (7) and (8) are strongly dependent on the laboratory setup since the standard uncertainties of tolerance, calibration, and resolution depend on the characteristics of the specific measuring devices used in the laboratory. Additionally, these uncertainty values depend on the rubber compound characteristics and manufacturing techniques. However, some trends in these results, such as the independence of the uncertainty β_{eff} with shear deformation level, compound type, or cycle selection, might also appear in isolators manufactured from different companies and should be further investigated.

The mean uncertainties, the uncertainty standard deviations, and the maximum observed uncertainties for all isolators in the dataset are summarized in Tables (10) to (13) for both effective properties (k_{eff} and β_{eff}), both manufacturing

compounds, and typical values of shear strain. Results are presented for the *scragged* and *unscragged* cases, i.e., averaging cycles 2 to 6 and 1 to 5, respectively.

Table 10 Expanded relative uncertainty in equivalent stiffness k_{eff}, considering only intercycle (Type A) uncertainty.

Averaging cycles 2 to 6								
	Compound 1				Compound 2			
Strain	$\overline{U}(\%)$	$\sigma_{U(\%)}$	$\max U(\%)$	N	$\overline{U}(\%)$	$\sigma_{U(\%)}$	$\max U(\%)$	N
$\boldsymbol{\gamma = 0.25}$	1.36	0.514	2.54	655	1.06	0.491	3.76	1163
$\boldsymbol{\gamma = 0.50}$	1.52	0.539	2.83	867	1.31	0.623	3.37	1106
$\boldsymbol{\gamma = 1.00}$	2.39	0.627	3.98	716	1.96	0.744	4.06	830
$\boldsymbol{\gamma = 1.50}$	2.55	0.537	4.41	284	1.85	0.329	2.55	136
Averaging cycles 1 to 5								
	Compound 1				Compound 2			
Strain	$\overline{U}(\%)$	$\sigma_{U(\%)}$	$\max U(\%)$	N	$\overline{U}(\%)$	$\sigma_{U(\%)}$	$\max U(\%)$	N
$\boldsymbol{\gamma = 0.25}$	2.64	0.986	5.03	655	1.93	1.011	7.43	1163
$\boldsymbol{\gamma = 0.50}$	2.91	0.914	5.34	867	2.38	1.251	5.68	1106
$\boldsymbol{\gamma = 1.00}$	4.48	1.161	7.16	716	3.51	1.627	7.63	830
$\boldsymbol{\gamma = 1.50}$	4.29	0.873	8.23	284	2.61	0.486	3.74	136

Table 11 Expanded relative uncertainty in equivalent damping β_{eff}, considering only intercycle (Type A) uncertainty.

Averaging cycles 2 to 6								
	Compound 1				Compound 2			
Strain	$\overline{U}(\%)$	$\sigma_{U(\%)}$	$\max U(\%)$	N	$\overline{U}(\%)$	$\sigma_{U(\%)}$	$\max U(\%)$	N
$\boldsymbol{\gamma = 0.25}$	1.17	0.621	4.53	655	1.19	0.724	5.87	1163
$\boldsymbol{\gamma = 0.50}$	1.34	0.730	3.34	867	1.21	0.714	3.66	1106
$\boldsymbol{\gamma = 1.00}$	2.21	0.844	4.46	716	1.58	0.914	4.42	830
$\boldsymbol{\gamma = 1.50}$	1.97	0.726	4.87	284	1.17	0.499	2.23	136
Averaging cycles 1 to 5								
	Compound 1				Compound 2			
Strain	$\overline{U}(\%)$	$\sigma_{U(\%)}$	$\max U(\%)$	N	$\overline{U}(\%)$	$\sigma_{U(\%)}$	$\max U(\%)$	N
$\boldsymbol{\gamma = 0.25}$	2.09	1.565	11.48	655	1.95	1.378	8.99	1163
$\boldsymbol{\gamma = 0.50}$	1.07	0.732	7.54	867	1.00	0.633	5.00	1106
$\boldsymbol{\gamma = 1.00}$	1.84	1.075	6.34	716	1.41	0.864	5.99	830
$\boldsymbol{\gamma = 1.50}$	2.41	0.967	5.21	284	0.98	0.508	2.51	136

Table 12 Expanded relative uncertainty in equivalent stiffness k_{eff}, considering intercycle uncertainty (Type A) and Type B uncertainty sources.

Averaging cycles 2 to 6								
	Compound 1				Compound 2			
Strain	$\overline{U}(\%)$	$\sigma_{U(\%)}$	$\max U(\%)$	N	$\overline{U}(\%)$	$\sigma_{U(\%)}$	$\max U(\%)$	N
$\boldsymbol{\gamma = 0.25}$	2.22	0.918	4.28	655	2.08	0.775	5.88	1163
$\boldsymbol{\gamma = 0.50}$	2.22	0.891	4.38	867	2.27	0.866	4.50	1106
$\boldsymbol{\gamma = 1.00}$	2.67	0.991	4.91	716	2.66	1.010	5.51	830
$\boldsymbol{\gamma = 1.50}$	3.16	0.891	5.19	284	2.73	0.793	4.20	136
Averaging cycles 1 to 5								
	Compound 1				Compound 2			
Strain	$\overline{U}(\%)$	$\sigma_{U(\%)}$	$\max U(\%)$	N	$\overline{U}(\%)$	$\sigma_{U(\%)}$	$\max U(\%)$	N
$\boldsymbol{\gamma = 0.25}$	2.94	1.247	6.33	655	2.41	1.146	5.97	1163
$\boldsymbol{\gamma = 0.50}$	3.37	1.299	6.48	867	2.95	1.037	6.07	1106

$\boldsymbol{\gamma = 1.00}$	4.88	1.310	7.90	716	4.49	1.907	9.26	830
$\boldsymbol{\gamma = 1.50}$	5.31	1.321	7.94	284	3.34	0.508	5.06	136

Table 13 Expanded relative uncertainty in equivalent damping $\boldsymbol{\beta_{eff}}$, considering intercycle uncertainty (Type A) and Type B uncertainty sources.

Averaging cycles 2 to 6								
	Compound 1				Compound 2			
Strain	$\bar{U}(\%)$	$\sigma_{U(\%)}$	$\max U(\%)$	N	$\bar{U}(\%)$	$\sigma_{U(\%)}$	$\max U(\%)$	N
$\boldsymbol{\gamma = 0.25}$	3.77	0.931	7.80	655	3.83	0.861	9.33	1163
$\boldsymbol{\gamma = 0.50}$	3.97	0.727	5.65	867	3.84	0.800	5.90	1106
$\boldsymbol{\gamma = 1.00}$	4.16	0.928	6.01	716	3.90	0.785	6.04	830
$\boldsymbol{\gamma = 1.50}$	3.89	0.812	6.06	284	3.62	0.787	4.64	136
Averaging cycles 1 to 5								
	Compound 1				Compound 2			
Strain	$\bar{U}(\%)$	$\sigma_{U(\%)}$	$\max U(\%)$	N	$\bar{U}(\%)$	$\sigma_{U(\%)}$	$\max U(\%)$	N
$\boldsymbol{\gamma = 0.25}$	3.77	1.268	12.18	655	3.65	1.087	9.41	1163
$\boldsymbol{\gamma = 0.50}$	3.32	0.788	6.27	867	3.40	0.729	6.90	1106
$\boldsymbol{\gamma = 1.00}$	3.77	1.081	7.58	716	3.19	0.958	7.11	830
$\boldsymbol{\gamma = 1.50}$	2.98	1.040	6.84	284	3.52	0.619	4.73	136

3.4 Sensitivity analysis of the uncertainty of $\boldsymbol{k_{eff}}$ and $\boldsymbol{\beta_{eff}}$

A comprehensive sensitivity analysis was performed, looking to determine which of the physically measured quantities (i.e., forces and displacements) has a stronger influence on the assessed uncertainties. In this analysis, different levels of Type-B uncertainties, ranging from 0% to 1%, were considered for forces and displacements. Subsequently, the *GUM* uncertainty quantification procedure was applied to the complete dataset of isolators' test results, combining these imposed Type-B uncertainties with the Type-A uncertainties inherent to the properties' random variability among cycles.

Figures (9) and (10) show contour maps of equal mean expanded relative uncertainty on k_{eff} and β_{eff} for the complete dataset, respectively. These dataset's mean values were evaluated under the assumption of a given Type-B standard relative uncertainty in the force (horizontal axis) and a given Type-B standard relative uncertainty in the displacement (vertical axis). For the sake of brevity, results are presented for the Compound 2 dataset, but similar trends were observed for Compound 1.

These figures enlighten some interesting facts. Figure (9) shows that for k_{eff} uncertainty assessment, the force measurement error, and the displacement measurement error are equally relevant, as the presented contour maps are circular-shaped. To reduce the uncertainty in k_{eff}, a reduction in the force measurement error or in the displacement measurement error will be equally effective. For example, to reduce the dataset mean stiffness expanded uncertainty from 2.8% to 2.2%, a reduction of 0.42% in the displacement measurement error is required. If the efforts are made in the force measurement error, a reduction of 0.46% shall be implemented. The contour curves for the low shear-strains levels, in subplots (a) and (b), are not that circular-shaped as the ones for the high shear-strains levels, subplots (c) and (d); however, the described dependencies still apply.

On the other hand, β_{eff} contour curves are contrastingly different from the ones of k_{eff}. The contour curves are almost vertical, for force uncertainties ranging from 0.4% to 1.0%, implying that the uncertainty in β_{eff} is strongly dependent on the force's measurement error and almost independent of the displacement's measurement error. For example, reducing the force's measurement error from 0.8% to 0.4% will reduce the expanded uncertainty of β_{eff} from 3.5% to 2.0%, regardless of the displacement error. On the other hand, reducing the displacement's measurement error from 0.8% to 0.4% will barely reduce the uncertainty in β_{eff} from 3.6% to 3.5% for a force Type-B uncertainty level of 0.8%, and from 2.4% to 2.0% for a force Type-B uncertainty level of 0.2%

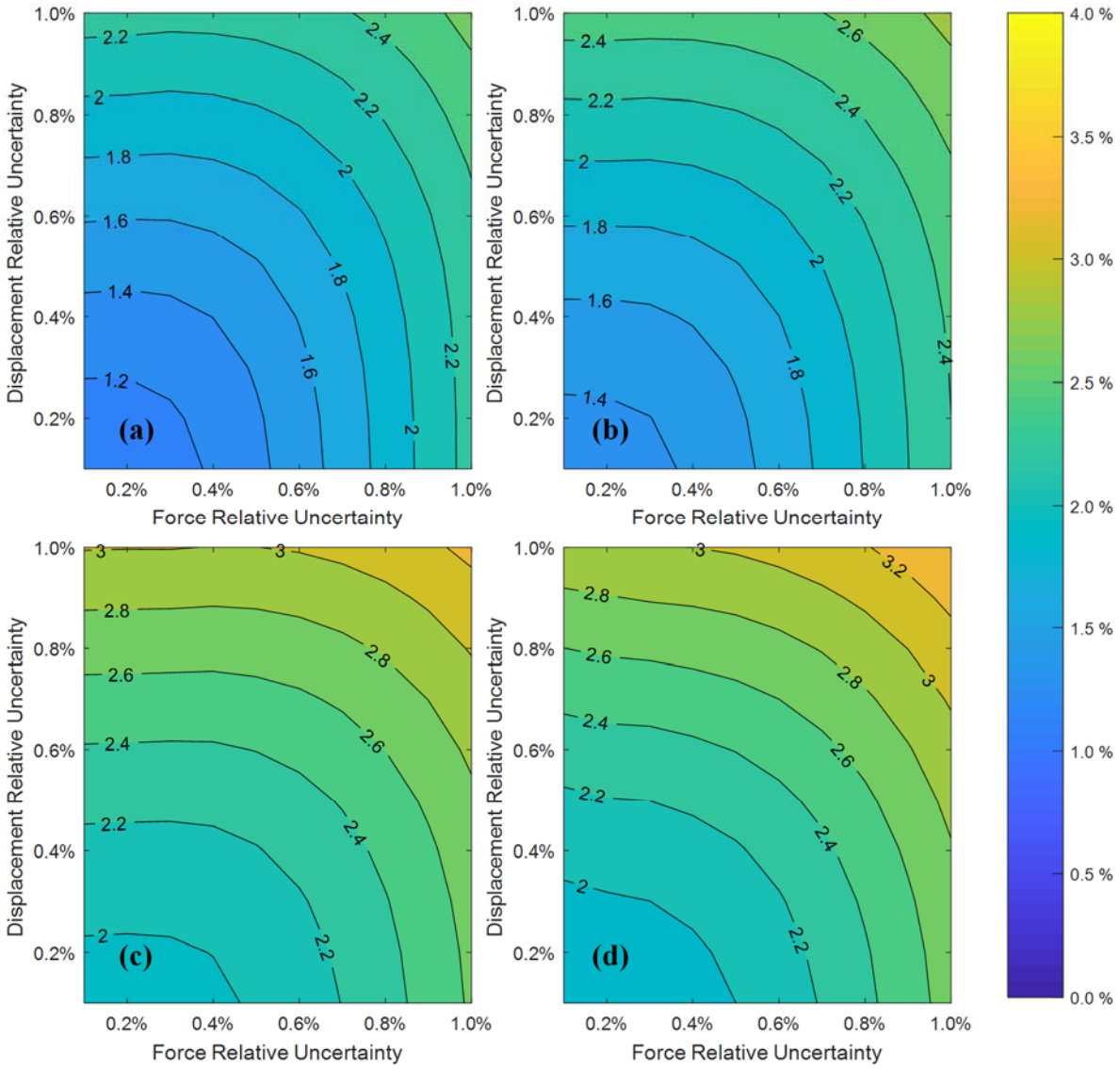

Figure 9. Contour curves of equal dataset mean expanded relative uncertainty of k_{eff} for different combinations of Type-B force relative uncertainty and Type-B displacement relative uncertainty for different levels of shear-strains: (a) $\gamma = 0.25$, (b) $\gamma = 0.50$, (c) $\gamma = 1.00$, and (d) $\gamma = 1.50$.

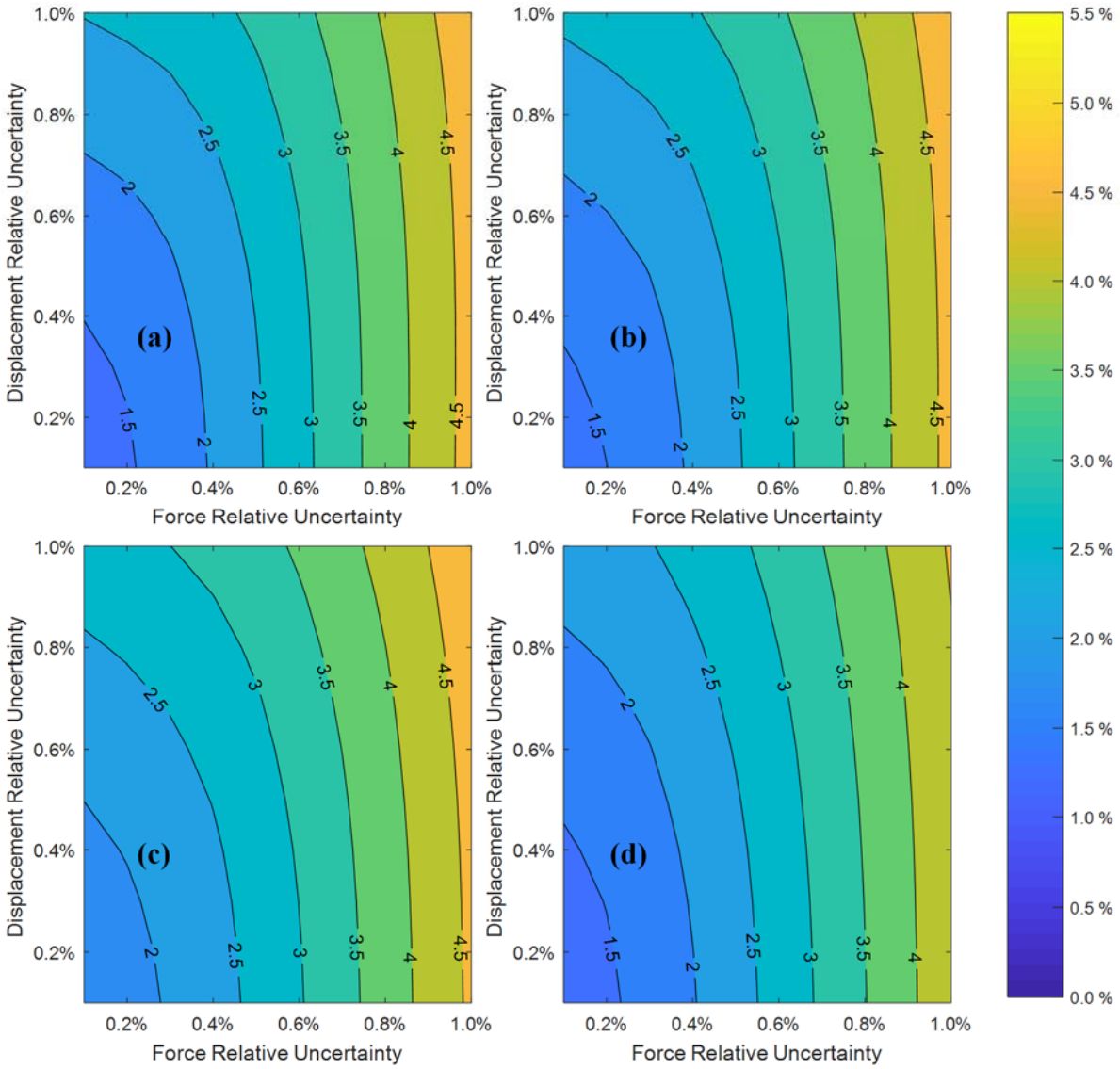

Figure 10. Contour curves of equal dataset mean expanded relative uncertainty of β_{eff} for different combinations of Type-B force relative uncertainty and Type-B displacement relative uncertainty for different levels of shear-strains: (a) $\gamma = 0.25$, (b) $\gamma = 0.50$, (c) $\gamma = 1.00$, and (d) $\gamma = 1.50$.

4. Conclusions

This research work has quantified and evaluated the uncertainty on the measured-by-test effective lateral stiffness and effective viscous damping ratio of a large dataset of 2,498 elastomeric seismic isolators, considering the methodology proposed by the *GUM* and using Monte-Carlo simulation. It is concluded that results from both approaches are, for all practical purposes, equivalent.

A thorough analysis of the seismic-code requirement of discarding the first deformation cycle to assess the *scragged* or *stable* properties was carried out. As it should be expected, stiffness results show that in the *unscragged* case, the mean and variability of the uncertainties are higher than those for the *scragged* case. On the other hand, there is no clear trend when comparing the uncertainties on the effective viscous damping for the *unscragged* and *scragged* cases, since the complete force-displacement hysteretic behavior is included in the uncertainty calculation, which reduces

the *scragging* influence. Mean relative-expanded uncertainties at the design shear strain for the *unscragged* case are 4.67% and 3.15% for effective lateral stiffness and for the effective viscous damping ratio, respectively. If the *scragged* cycles are considered, these values change to 3.02% and 3.80%, respectively.

If repeatability is considered as the only source of uncertainty (Type A), the dataset maximum relative-expanded uncertainty values are 8% and 11% for the effective stiffness and the effective viscous damping, respectively. The addition of Type B uncertainty sources increases these values to 9% and 12%, respectively.

A sensitivity analysis to evaluate the relevance of the directly-measured input quantities (i.e., forces and displacements) in the effective properties uncertainties was performed. Generally speaking, it could be stated that in stiffness uncertainty assessment, the force and displacement measurements are equally relevant. On the other hand, in damping uncertainty assessment, the force measurements are significantly more relevant than the displacement ones. To improve the measurands' quality, efforts should be made to reduce the error in force measurements rather than in displacement measurements.

Finally, it was proven that for the approach used to assess the effective stiffness and the effective viscous damping uncertainties, the first-order Taylor approximation is sufficiently accurate in this case where variabilities are relatively small. Moreover, differences between uncertainties calculated with *GUM* first-order approximation, *GUM* second-order approximation, and Monte-Carlo simulations, considering correlated input variables, were found to be negligible.

Acknowledgments

This research was funded by CONICYT Doctorado Nacional 21161027, the National Research Center for Integrated Natural Disaster Management CONICYT /FONDAP/15110017, and CONICYT/FONDECYT/1170836. The authors also would like to thank the John A. Blume Earthquake Engineering Center at Stanford University for hosting the first author during his one-year stay at Stanford as visiting student researcher.

References

1. American Society of Civil Engineers (ASCE). *Minimum Design Loads for Buildings and Other Structures, ASCE/SEI 7-16*. 2017.
2. Instituto Nacional de Normalización (INN). *NCh2745.Of2013 - Análisis y diseño de Edificios con Aislación Sísmica (In Spanish)*. 2013.
3. Mullins L. Softening of rubber by displacement. *Rubber Chemistry and Technology* 1969; **42**(1): 339–362.
4. American Society of Civil Engineers (ASCE). *Minimum Design Loads for Buildings and Other Structures, ASCE/SEI 7−16*.
5. Anil K. Chopra. *Dynamics of Structures Theory and Applications to Earthquake Engineering*. Fourth Edi. Prentice Hall; 2012.
6. BIPM, IEC, IFCC, ILAC, ISO, IUPAC I and O. International Vocabulary of Metrology - Basic and General Concepts and Associated Terms (VIM), JCGM 200:2012. *International Organization for Standardization Geneva ISBN* 2012(Vim): 104. DOI: 10.1016/0263-2241(85)90006-5.
7. Birge RT. The Propagation of Errors. *American Journal of Physics* 1939; **7**(6): 351–357. DOI: 10.1119/1.1991484.
8. BIPM, IEC, IFCC, ILAC, ISO, IUPAC I and O. Guide to the Expression of Uncertainty in Measurement, JCGM 100:2008 (GUM 1995 with minor corrections). *International Organization for Standardization Geneva ISBN* 2008.
9. Stant LT, Aaen PH, Ridler NM. Comparing methods for evaluating measurement uncertainty given in the JCGM' Evaluation of Measurement Data' documents. *Measurement: Journal of the International Measurement Confederation* 2016; **94**(2016): 847–851. DOI: 10.1016/j.measurement.2016.08.015.
10. BIPM, IEC, IFCC, ILAC, ISO, IUPAC I and O. Supplement 1 to the "Guide to the Expression of Uncertainty in Measurement" - Propagation of distributions using a Monte Carlo method, JCGM 101:2008. *International Organization for Standardization Geneva ISBN* 2008.
11. Da Silva Hack P, Ten Caten CS. Measurement uncertainty: Literature review and research trends. *IEEE Transactions on Instrumentation and Measurement* 2012; **61**(8): 2116–2124. DOI: 10.1109/TIM.2012.2193694.

12. Mauris G, Lasserre V, Foulloy L. A fuzzy approach for the expression of uncertainty in measurement. *Measurement: Journal of the International Measurement Confederation* 2001; **29**(3): 165–177. DOI: 10.1016/S0263-2241(00)00036-1.
13. Ferrero A, Salicone S. The random-fuzzy variables: A new approach to the expression of uncertainty in measurement. *IEEE Transactions on Instrumentation and Measurement* 2004; **53**(5): 1370–1377. DOI: 10.1109/TIM.2004.831506.
14. Shahanaghi K, Nakhjiri P. A new optimized uncertainty evaluation applied to the Monte-Carlo simulation in platinum resistance thermometer calibration. *Measurement: Journal of the International Measurement Confederation* 2010; **43**(7): 901–911. DOI: 10.1016/j.measurement.2010.03.008.
15. Theodorou D, Meligotsidou L, Karavoltsos S, Burnetas A, Dassenakis M, Scoullos M. Comparison of ISO-GUM and Monte Carlo methods for the evaluation of measurement uncertainty: Application to direct cadmium measurement in water by GFAAS. *Talanta* 2011; **83**(5): 1568–1574. DOI: 10.1016/j.talanta.2010.11.059.
16. Chen A, Chen C. Comparison of GUM and Monte Carlo methods for evaluating measurement uncertainty of perspiration measurement systems. *Measurement: Journal of the International Measurement Confederation* 2016; **87**: 27–37. DOI: 10.1016/j.measurement.2016.03.007.
17. Junga R, Chudy P, Pospolita J. Uncertainty estimation of the efficiency of small-scale boilers. *Measurement: Journal of the International Measurement Confederation* 2017; **97**: 186–194. DOI: 10.1016/j.measurement.2016.11.011.
18. Moona G, Sharma R, Kumar H. Evaluation of uncertainty of measurement of shadow mask dot pitch using different approaches. *Transactions of the Institute of Measurement and Control* 2018; **40**(7): 2428–2435. DOI: 10.1177/0142331217707367.
19. Tutmez B, Baranovskii A. Quantifying uncertainty in railway noise measurement. *Measurement: Journal of the International Measurement Confederation* 2019; **137**: 1–6. DOI: 10.1016/j.measurement.2019.01.024.
20. Link A, Täubner A, Wabinski W, Bruns T, Elster C. Modelling accelerometers for transient signals using calibration measurements upon sinusoidal excitation. *Measurement: Journal of the International Measurement Confederation* 2007; **40**(9–10): 928–935. DOI: 10.1016/j.measurement.2006.10.011.
21. Bringmann B, Knapp W. Machine tool calibration: Geometric test uncertainty depends on machine tool performance. *Precision Engineering* 2009; **33**(4): 524–529. DOI: 10.1016/j.precisioneng.2009.02.002.
22. Leyi G, Wei Z, Jing Z, Songling H. Mechanics analysis and simulation of material Brinell hardness measurement. *Measurement: Journal of the International Measurement Confederation* 2011; **44**(10): 2129–2137. DOI: 10.1016/j.measurement.2011.07.024.
23. Mahmoud GM, Hegazy RS. Comparison of GUM and Monte Carlo methods for the uncertainty estimation in hardness measurements. *International Journal of Metrology and Quality Engineering* 2017; **8**: 1–9. DOI: 10.1051/ijmqe/2017014.
24. Kuhinek D, Zorić I, Hrženjak P. Measurement uncertainty in testing of uniaxial compressive strength and deformability of rock samples. *Measurement Science Review* 2011. DOI: 10.2478/v10048-011-0021-2.
25. Tutmez B. Measurement uncertainty analysis for compressive loading-based ultrasonic wave propagation. *Nondestructive Testing and Evaluation* 2017; **32**(3): 269–285. DOI: 10.1080/10589759.2016.1200575.
26. Godina A, Acko B. Measurement uncertainty analysis for calibration of gauge blocks. *Procedia Engineering* 2014; **69**: 191–198. DOI: 10.1016/j.proeng.2014.02.220.
27. Salah B, Slimane Z, Zoheir M, Jurgen B. Uncertainty estimation of mechanical testing properties using sensitivity analysis and stochastic modelling. *Measurement: Journal of the International Measurement Confederation* 2015; **62**: 149–154. DOI: 10.1016/j.measurement.2014.10.036.
28. Fabricio DAK, Hack P da S, Caten CS ten. Estimation of the measurement uncertainty in the anisotropy test. *Measurement: Journal of the International Measurement Confederation* 2016; **93**: 303–309. DOI: 10.1016/j.measurement.2016.07.027.
29. De la Llera JC, Luders C, Leigh P, Sady H. Analysis, testing, and implementation of seismic isolation of buildings in Chile. *Earthquake Engineering and Structural Dynamics* 2004; **33**(5): 543–574. DOI: 10.1002/eqe.360.
30. Lira I. *Evaluating the Measurement Uncertainty: Fundamentals and Practical Guidance*. 2002.
31. Mekid S, Vaja D. Propagation of uncertainty: Expressions of second and third order uncertainty with third and fourth moments. *Measurement: Journal of the International Measurement Confederation* 2008; **41**(6): 600–609. DOI: 10.1016/j.measurement.2007.07.004.
32. MTS System Corporation. *Certificate of Calibration, SN10320683:1280148971*. 2010.
33. MTS System Corporation. *Certificate of Calibration, ACT3-182*. 2010.

34. Willink R. A generalization of the Welch-Satterthwaite formula for use with correlated uncertainty components. *Metrologia* 2007; **44**(5): 340–349. DOI: 10.1088/0026-1394/44/5/010.
35. Tubaldi E, Ragni L, Dall'Asta A, Ahmadi H, Muhr A. Stress softening behaviour of HDNR bearings: modelling and influence on the seismic response of isolated structures. *Earthquake Engineering and Structural Dynamics* 2017. DOI: 10.1002/eqe.2897.

Appendix A

The expression for the uncertainty propagation using a second-order Taylor approximation is derived as follows:

A second-order approximation of a function $y = f(x_1, x_2, \dots, x_n)$ can be written as

$$y\,(x_1, x_2, \dots, x_n) = y\,(\bar{x}_1, \bar{x}_2, \dots, \bar{x}_n) + \sum_{i=1}^{n} \frac{\partial y}{\partial x_i}(x_i - \bar{x}_i) + \frac{1}{2}\sum_{i=1}^{n} \frac{\partial^2 y}{\partial {x_i}^2}(x_i - \bar{x}_i)^2 \tag{A-1}$$

Applying the expectation operator

$$E[y\,(x_1, x_2, \dots, x_n)] = \bar{y} = E\left[y\,(\bar{x}_1, \bar{x}_2, \dots, \bar{x}_n) + \sum_{i=1}^{n} \frac{\partial y}{\partial x_i}(x_i - \bar{x}_i) + \frac{1}{2}\sum_{i=1}^{n} \frac{\partial^2 y}{\partial {x_i}^2}(x_i - \bar{x}_i)^2 \right] \tag{A-2}$$

The first term in the right side of the equation is constant and the second term vanishes to zero as it includes the term $E(x_i - \bar{x}_i)$, then rewriting equation (A-2) gives:

$$\bar{y} = y\,(\bar{x}_1, \bar{x}_2, \dots, \bar{x}_n) + \frac{1}{2}\sum_{i=1}^{n} \frac{\partial^2 y}{\partial {x_i}^2} E[(x_i - \bar{x}_i)^2] \tag{A-3}$$

Subtracting equation (A-3) from (A-1) gives:

$$y - \bar{y} = \sum_{i=1}^{n} \frac{\partial y}{\partial x_i}(x_i - \bar{x}_i) + \frac{1}{2}\sum_{i=1}^{n} \frac{\partial^2 y}{\partial {x_i}^2}(x_i - \bar{x}_i)^2 - \frac{1}{2}\sum_{i=1}^{n} \frac{\partial^2 y}{\partial {x_i}^2} E[(x_i - \bar{x}_i)^2] \tag{A-4}$$

Squaring equation (A-4):

$$(y - \bar{y})^2 = \left[\sum_{i=1}^{n} \frac{\partial y}{\partial x_i}(x_i - \bar{x}_i) + \frac{1}{2}\sum_{i=1}^{n} \frac{\partial^2 y}{\partial {x_i}^2}(x_i - \bar{x}_i)^2 - \frac{1}{2}\sum_{i=1}^{n} \frac{\partial^2 y}{\partial {x_i}^2} E[(x_i - \bar{x}_i)^2] \right]^2 \tag{A-5}$$

Expanding the right side of the equation gives:

$$\begin{aligned} (y - \bar{y})^2 = {} & \left[\sum_{i=1}^{n} \frac{\partial y}{\partial x_i}(x_i - \bar{x}_i) \right]^2 + \left[\frac{1}{2}\sum_{i=1}^{n} \frac{\partial^2 y}{\partial {x_i}^2}(x_i - \bar{x}_i)^2 \right]^2 + \left[\frac{1}{2}\sum_{i=1}^{n} \frac{\partial^2 y}{\partial {x_i}^2} E[(x_i - \bar{x}_i)^2] \right]^2 \\ & + 2\left[\sum_{i=1}^{n} \frac{\partial y}{\partial x_i}(x_i - \bar{x}_i) \right]\left[\frac{1}{2}\sum_{i=1}^{n} \frac{\partial^2 y}{\partial {x_i}^2}(x_i - \bar{x}_i)^2 \right] \\ & + 2\left[\sum_{i=1}^{n} \frac{\partial y}{\partial x_i}(x_i - \bar{x}_i) \right]\left[-\frac{1}{2}\sum_{i=1}^{n} \frac{\partial^2 y}{\partial {x_i}^2} E[(x_i - \bar{x}_i)^2] \right] \\ & + 2\left[\frac{1}{2}\sum_{i=1}^{n} \frac{\partial^2 y}{\partial {x_i}^2}(x_i - \bar{x}_i)^2 \right]\left[-\frac{1}{2}\sum_{i=1}^{n} \frac{\partial^2 y}{\partial {x_i}^2} E[(x_i - \bar{x}_i)^2] \right] \end{aligned} \tag{A-6}$$

Applying the expectation operator gives and simplifying some terms:

$$
\begin{aligned}
E[(y-\bar{y})^2] = {} & E\left(\left[\sum_{i=1}^{n}\frac{\partial y}{\partial x_i}(x_i-\bar{x}_i)\right]^2\right)+E\left(\left[\frac{1}{2}\sum_{i=1}^{n}\frac{\partial^2 y}{\partial {x_i}^2}(x_i-\bar{x}_i)^2\right]^2\right) \\
& +E\left(\left[\frac{1}{2}\sum_{i=1}^{n}\frac{\partial^2 y}{\partial {x_i}^2}E[(x_i-\bar{x}_i)^2]\right]^2\right)+E\left(\left[\sum_{i=1}^{n}\frac{\partial y}{\partial x_i}(x_i-\bar{x}_i)\right]\left[\sum_{i=1}^{n}\frac{\partial^2 y}{\partial {x_i}^2}(x_i-\bar{x}_i)^2\right]\right) \\
& -E\left(\left[\sum_{i=1}^{n}\frac{\partial y}{\partial x_i}(x_i-\bar{x}_i)\right]\left[\sum_{i=1}^{n}\frac{\partial^2 y}{\partial {x_i}^2}E[(x_i-\bar{x}_i)^2]\right]\right) \\
& -E\left(\left[\frac{1}{2}\sum_{i=1}^{n}\frac{\partial^2 y}{\partial {x_i}^2}(x_i-\bar{x}_i)^2\right]\left[\sum_{i=1}^{n}\frac{\partial^2 y}{\partial {x_i}^2}E[(x_i-\bar{x}_i)^2]\right]\right)
\end{aligned}
\tag{A-7}
$$

The fifth term in the right side vanishes to zero because when the product of the summations is expanded, each term includes a $E(x_i-\bar{x}_i)$ term. For convenience, the expectation operator in the last term is interchanged with the summation operator. Rewriting gives:

$$
\begin{aligned}
E[(y-\bar{y})^2] = {} & E\left(\left[\sum_{i=1}^{n}\frac{\partial y}{\partial x_i}(x_i-\bar{x}_i)\right]^2\right)+\frac{1}{4}E\left(\left[\sum_{i=1}^{n}\frac{\partial^2 y}{\partial {x_i}^2}(x_i-\bar{x}_i)^2\right]^2\right) \\
& +\frac{1}{4}E\left(\left[\sum_{i=1}^{n}\frac{\partial^2 y}{\partial {x_i}^2}E[(x_i-\bar{x}_i)^2]\right]^2\right)+E\left(\left[\sum_{i=1}^{n}\frac{\partial y}{\partial x_i}(x_i-\bar{x}_i)\right]\left[\sum_{i=1}^{n}\frac{\partial^2 y}{\partial {x_i}^2}(x_i-\bar{x}_i)^2\right]\right) \\
& -\frac{1}{2}\left(\left[\sum_{i=1}^{n}\frac{\partial^2 y}{\partial {x_i}^2}E(x_i-\bar{x}_i)^2\right]\left[\sum_{i=1}^{n}\frac{\partial^2 y}{\partial {x_i}^2}E[(x_i-\bar{x}_i)^2]\right]\right)
\end{aligned}
\tag{A-8}
$$

It should be noted that in the third term, all the addends are constant, then the outside expectation operator does not have any effect. Then it turns out that the third and the fifth terms can be reduced to a unique term.

$$
\begin{aligned}
E[(y-\bar{y})^2] = {} & E\left(\left[\sum_{i=1}^{n}\frac{\partial y}{\partial x_i}(x_i-\bar{x}_i)\right]^2\right)+\frac{1}{4}E\left(\left[\sum_{i=1}^{n}\frac{\partial^2 y}{\partial {x_i}^2}(x_i-\bar{x}_i)^2\right]^2\right) \\
& +E\left(\left[\sum_{i=1}^{n}\frac{\partial y}{\partial x_i}(x_i-\bar{x}_i)\right]\left[\sum_{i=1}^{n}\frac{\partial^2 y}{\partial {x_i}^2}(x_i-\bar{x}_i)^2\right]\right)-\frac{1}{4}\left[\sum_{i=1}^{n}\frac{\partial^2 y}{\partial {x_i}^2}E[(x_i-\bar{x}_i)^2]\right]^2
\end{aligned}
\tag{A-9}
$$

The four terms in equation (A-9) are expanded and written in a more convenient matrix format. Then the first term gives:

$$
\begin{aligned}
& E\left(\left[\sum_{i=1}^{n}\frac{\partial y}{\partial x_i}(x_i-\bar{x}_i)\right]^2\right) \\
& \quad =\sum_{i=1}^{n}\left(\frac{\partial y}{\partial x_i}\right)^2 E[(x_i-\bar{x}_i)^2] \\
& \quad +2\sum_{i=1}^{n-1}\sum_{j=i+1}^{n}\frac{\partial y}{\partial x_i}\frac{\partial y}{\partial x_j}E\big[(x_i-\bar{x}_i)\big(x_j-\bar{x}_j\big)\big]=\boldsymbol{g^T\,cov(x_i)\,g}
\end{aligned}
\tag{A-10}
$$

where

$$\boldsymbol{g} = \left[\frac{\partial y}{\partial x_1} \quad \frac{\partial y}{\partial x_2} \quad \dots \quad \frac{\partial y}{\partial x_n}\right]^{\boldsymbol{T}} \tag{A-11}$$

and

$$\boldsymbol{cov}(\boldsymbol{x_i}) = \begin{bmatrix} u^2(x_1) & r(x_1,x_2)\,u(x_1)\,u(x_2) & \dots & r(x_1,x_n)\,u(x_1)\,u(x_n) \\ r(x_2,x_1)\,u(x_2)\,u(x_1) & u^2(x_2) & \dots & r(x_2,x_n)\;u(x_2)\,u(x_n) \\ \vdots & \vdots & \ddots & \vdots \\ r(x_n,x_1)\,u(x_n)\,u(x_1) & r(x_n,x_2)\,u(x_n)\,u(x_2) & \dots & u^2(x_n) \end{bmatrix} \tag{A-12}$$

The second term turns into:

$$\begin{aligned} &\frac{1}{4}E\left(\left[\sum_{i=1}^{n}\frac{\partial^2 y}{\partial {x_i}^2}(x_i-\bar{x}_i)^2\right]^2\right) \\ &\qquad = \frac{1}{4}\sum_{i=1}^{n}\left(\frac{\partial^2 y}{\partial {x_i}^2}\right)^2 E[(x_i-\bar{x}_i)^4] \\ &\qquad + \left(\frac{1}{4}\right)(2)\sum_{i=1}^{n-1}\sum_{j=i+1}^{n}\frac{\partial^2 y}{\partial {x_i}^2}\frac{\partial^2 y}{\partial {x_j}^2}E\left[(x_i-\bar{x}_i)^2\left(x_j-\bar{x}_j\right)^2\right] = \frac{1}{4}(\boldsymbol{g'})^{\boldsymbol{T}}\,\boldsymbol{krt}(\boldsymbol{x_i})\,\boldsymbol{g'} \end{aligned} \tag{A-13}$$

where

$$\boldsymbol{g'} = \left[\frac{\partial^2 y}{\partial {x_1}^2} \quad \frac{\partial^2 y}{\partial {x_2}^2} \quad \dots \quad \frac{\partial^2 y}{\partial {x_n}^2}\right] \tag{A-14}$$

and

$$\boldsymbol{krt}(\boldsymbol{x_i}) = \boldsymbol{E}\begin{bmatrix} (x_1-\bar{x}_1)^4 & (x_1-\bar{x}_1)^2(x_2-\bar{x}_2)^2 & \dots & (x_1-\bar{x}_1)^2(x_n-\bar{x}_n)^2 \\ (x_2-\bar{x}_2)^2(x_1-\bar{x}_1)^2 & (x_2-\bar{x}_2)^4 & \dots & (x_2-\bar{x}_2)^2(x_n-\bar{x}_n)^2 \\ \vdots & \vdots & \ddots & \vdots \\ (x_n-\bar{x}_n)^2(x_1-\bar{x}_1)^2 & (x_n-\bar{x}_n)^2(x_2-\bar{x}_2)^2 & \dots & (x_n-\bar{x}_n)^4 \end{bmatrix} \tag{A-15}$$

When expanding the third term it gives:

$$\begin{aligned} &E\left(\left[\sum_{i=1}^{n}\frac{\partial y}{\partial x_i}(x_i-\bar{x}_i)\right]\left[\sum_{i=1}^{n}\frac{\partial^2 y}{\partial {x_i}^2}(x_i-\bar{x}_i)^2\right]\right) \\ &\qquad = \sum_{i=1}^{n}\left(\frac{\partial y}{\partial x_i}\right)\left(\frac{\partial^2 y}{\partial {x_i}^2}\right)E[(x_i-\bar{x}_i)^3] \\ &\qquad + \sum_{i=1}^{n}\sum_{\substack{j\neq i \\ j=1}}^{n}\left(\frac{\partial y}{\partial x_i}\right)\left(\frac{\partial^2 y}{\partial {x_j}^2}\right)E\left[(x_i-\bar{x}_i)\left(x_j-\bar{x}_j\right)^2\right] = (\boldsymbol{g})^{\boldsymbol{T}}\,\boldsymbol{skw}(\boldsymbol{x_i})\,\boldsymbol{g'} \end{aligned} \tag{A-16}$$

where $\boldsymbol{g}$ and $\boldsymbol{g'}$ were defined in equations (A-11) and (A-14) respectively and:

$$\boldsymbol{skw}(\boldsymbol{x_i}) = \boldsymbol{E}\begin{bmatrix} (x_1-\bar{x}_1)^3 & (x_1-\bar{x}_1)(x_2-\bar{x}_2)^2 & \dots & (x_1-\bar{x}_1)(x_n-\bar{x}_n)^2 \\ (x_2-\bar{x}_2)(x_1-\bar{x}_1)^2 & (x_2-\bar{x}_2)^3 & \dots & (x_2-\bar{x}_2)(x_n-\bar{x}_n)^2 \\ \vdots & \vdots & \ddots & \vdots \\ (x_n-\bar{x}_n)(x_1-\bar{x}_1)^2 & (x_n-\bar{x}_n)(x_2-\bar{x}_2)^2 & \dots & (x_n-\bar{x}_n)^3 \end{bmatrix} \tag{A-17}$$

Finally, the fourth term can be expanded as shown:

$$\begin{aligned} \frac{1}{4}\left[\sum_{i=1}^{n}\frac{\partial^2 y}{\partial {x_i}^2}E[(x_i-\bar{x}_i)^2]\right]^2 &= \frac{1}{4}\left[\sum_{i=1}^{n}\frac{\partial^2 y}{\partial {x_i}^2}u^2(x_i)\right]^2 \\ &= \frac{1}{4}\sum_{i=1}^{n}\left(\frac{\partial^2 y}{\partial {x_i}^2}\right)^2 (u^2(x_i))^2 \\ &+ \left(\frac{1}{4}\right)(2)\sum_{i=1}^{n-1}\sum_{j=i+1}^{n}\left(\frac{\partial^2 y}{\partial {x_i}^2}\right)\left(\frac{\partial^2 y}{\partial {x_j}^2}\right)u^2(x_i)\,u^2(x_j) \;= \frac{1}{4}\boldsymbol{g'^T}\,\boldsymbol{Var^2}(\boldsymbol{x_i})\,\boldsymbol{g'} \end{aligned} \tag{A-18}$$

where

$$\boldsymbol{Var^2}(\boldsymbol{x_i}) = \begin{bmatrix} u^4(x_1) & u^2(x_1)u^2(x_2) & \dots & u^2(x_1)u^2(x_n) \\ u^2(x_2)u^2(x_1) & u^4(x_2) & \dots & u^2(x_2)u^2(x_n) \\ \vdots & \vdots & \ddots & \vdots \\ u^2(x_n)u^2(x_1) & u^2(x_n)u^2(x_2) & \dots & u^4(x_n) \end{bmatrix} \tag{A-19}$$

Rewriting equation (A-9) in compact matrix format gives:

$$\boldsymbol{Var}(\boldsymbol{y}) = \boldsymbol{g^T}\,\boldsymbol{cov}(\boldsymbol{x_i})\,\boldsymbol{g} + \frac{1}{4}(\boldsymbol{g'})^{\boldsymbol{T}}\,\boldsymbol{krt}(\boldsymbol{x_i})\,\boldsymbol{g'} + (\boldsymbol{g})^{\boldsymbol{T}}\,\boldsymbol{skw}(\boldsymbol{x_i})\,\boldsymbol{g'} - \frac{1}{4}\boldsymbol{g'^T}\,\boldsymbol{Var^2}(\boldsymbol{x_i})\,\boldsymbol{g'} \tag{A-20}$$

Equation that was implemented in the presented manuscript.

Appendix B

The second derivatives required to evaluate equations (11) and (15) are shown in Appendix B

$$\frac{\partial^2 k_{eff}}{\partial F^{+2}} = 0 \tag{B-1}$$

$$\frac{\partial^2 k_{eff}}{\partial F^{-2}} = 0 \tag{B-2}$$

$$\frac{\partial^2 k_{eff}}{\partial \Delta^{+2}} = \frac{2(\mathrm{F}^+ - \mathrm{F}^-)}{(\Delta^+ - \Delta^-)^3} \tag{B-3}$$

$$\frac{\partial^2 k_{eff}}{\partial \Delta^{-2}} = \frac{2(\mathrm{F}^+ - \mathrm{F}^-)}{(\Delta^+ - \Delta^-)^3} \tag{B-4}$$

$$\frac{\partial^2 \beta_{eff}}{\partial {E_{loop}}^2} = 0 \tag{B-5}$$

$$\frac{\partial^2 \beta_{eff}}{\partial {k_{eff}}^2} = \frac{4}{\pi} \frac{E_{loop}}{{k_{eff}}^3 (\Delta^+ - \Delta^-)^2} \tag{B-6}$$

$$\frac{\partial^2 \beta_{eff}}{\partial \Delta^{+2}} = \frac{-12}{\pi} \frac{E_{loop}}{k_{eff} (\Delta^+ - \Delta^-)^4} \tag{B-7}$$

$$\frac{\partial^2 \beta_{eff}}{\partial {k_{eff}}^2} = \frac{12}{\pi} \frac{E_{loop}}{k_{eff} (\Delta^+ - \Delta^-)^4} \tag{B-8}$$